



**HAL**  
open science

## **New geological and geochronological constraints on the evolution of the Cotacachi - Cuicocha volcanic complex (Ecuador)**

Marco Almeida Vaca, Mathilde Bablon, S. Daniel Andrade, Silvana Hidalgo, Xavier Quidelleur, Francisco Vasconez, Anais Vásconez Müller, Pierre Lahitte, Pablo Samaniego

### ► To cite this version:

Marco Almeida Vaca, Mathilde Bablon, S. Daniel Andrade, Silvana Hidalgo, Xavier Quidelleur, et al.. New geological and geochronological constraints on the evolution of the Cotacachi - Cuicocha volcanic complex (Ecuador). *Journal of South American Earth Sciences*, 2023, 128, pp.104489. 10.1016/j.jsames.2023.104489 . hal-04166917

**HAL Id: hal-04166917**

**<https://hal.science/hal-04166917v1>**

Submitted on 1 Dec 2023

**HAL** is a multi-disciplinary open access archive for the deposit and dissemination of scientific research documents, whether they are published or not. The documents may come from teaching and research institutions in France or abroad, or from public or private research centers.

L'archive ouverte pluridisciplinaire **HAL**, est destinée au dépôt et à la diffusion de documents scientifiques de niveau recherche, publiés ou non, émanant des établissements d'enseignement et de recherche français ou étrangers, des laboratoires publics ou privés.

1 **New geological and geochronological constraints on the evolution of the Cotacachi**  
2 **- Cuicocha Volcanic Complex (Ecuador)**

3 *Marco Almeida Vaca<sup>1</sup>, Mathilde Bablon<sup>2,3</sup>, S. Daniel Andrade<sup>1</sup>, Silvana Hidalgo<sup>1</sup>, Xavier Quidelleur<sup>2</sup>,*  
4 *Francisco J. Vasconez<sup>1</sup>, Anaïs Vásconez Müller<sup>1</sup>, Pierre Lahitte<sup>2</sup>, Pablo Samaniego<sup>4</sup>*

5 <sup>1</sup> *Instituto Geofísico, Escuela Politécnica Nacional, Ap. 17-01-2759, Quito, Ecuador.*

6 <sup>2</sup> *Université Paris-Saclay, CNRS, GEOPS, Orsay, 91405, France.*

7 <sup>3</sup> *Université Côte d'Azur, CNRS, IRD, Observatoire de la Côte d'Azur, Géoazur, Valbonne, France*

8 <sup>4</sup> *Laboratoire Magmas et Volcans, Université Clermont Auvergne - CNRS - IRD, 6 Avenue Blaise Pascal, 63178*  
9 *Aubière, France.*

10 **Abstract**

11 Extensive fieldwork at the Cotacachi-Cuicocha Volcanic Complex (CCVC, North of  
12 Ecuador) resulted in a new collection of geological data including cartography,  
13 chronology, petrography, geochemistry, and morphology. This volcanic complex is  
14 formed by a central volcano (Cotacachi: 4939 m asl, current bulk volume of  $56 \pm 4$   
15  $\text{km}^3$ ), several peripheral domes, and a 3 km wide volcanic caldera (Cuicocha:  $4.2 \pm$   
16  $0.1 \text{ km}^3$ ). CCVC comprises three stratigraphic members: The first, Cotacachi Basal,  
17 represents the initial phase of construction, which started at  $173 \pm 4 \text{ ka}$  with a basal  
18 andesitic lava flow succession (~500 m-thick) including isolated basaltic-andesitic  
19 lavas (Verde Tola unit; NE:  $113 \pm 6 \text{ ka}$ , SE:  $133 \pm 9 \text{ ka}$ ), the construction of some  
20 peripheral amphibole-bearing andesitic domes, such as Muyurcu and Loma Negra  
21 ( $138 \pm 4 \text{ ka}$  and  $<108 \text{ ka}$ , respectively), and a debris-avalanche deposit to the north-  
22 west ( $0.5 - 1.8 \text{ km}^3$ , older than 108 ka). The second member, Upper Cotacachi,  
23 consists of an andesitic lava flow succession (~300 m-thick), younger than  $108 \pm 6$   
24 ka. A gap of activity occurred afterwards from 100 to 70 ka, during which a second  
25 debris-avalanche ( $0.2 - 1.1 \text{ km}^3$ , 108 to 65 ka) occurred to the NE, followed by the  
26 effusion of the dacitic Piribuela dome ( $65 \pm 2 \text{ ka}$ ). Afterwards, several superimposed  
27 andesitic lava flows were emplaced at the summit, possibly around 15 - 10 ka since  
28 they lack glacial erosion. The third member includes the extrusion of the andesitic  
29 Cuicocha pre-caldera domes, which marks the beginning of a new eruptive stage of  
30 activity of CCVC during the Holocene, resulting in a violent eruption ( $3525 \pm 35$  to  
31  $2980 \pm 30 \text{ a BP}$ ; VEI= 5) that partially destroyed the young dome and formed a  
32 funnel-shaped caldera (Cuicocha Caldera-Lake), ending with the emplacement of  
33 the Wolf and Yerovi post-caldera domes.

## 34 1. INTRODUCTION

35 The Cotacachi-Cuicocha Volcanic Complex (CCVC: 0.361°N, 78. 349°W), one of  
36 the largest volcanic centres in the northern part of the Ecuadorian Andes, is located  
37 ~50 km north of Quito. Its southern flanks are covered by pyroclastic deposits related  
38 to the Cuicocha caldera-forming eruption, which is one of the most explosive events  
39 to have occurred in the Ecuadorian volcanic arc during the Holocene (von  
40 Hillebrandt, 1989; Hall and Mothes, 1994; Pidgen, 2014). Highly populated (approx.  
41 thirteen thousand inhabitants - [https://www.ecuadorencifras.gob.ec/base-de-datos-](https://www.ecuadorencifras.gob.ec/base-de-datos-censo-de-poblacion-y-vivienda/)  
42 [censo-de-poblacion-y-vivienda/](https://www.ecuadorencifras.gob.ec/base-de-datos-censo-de-poblacion-y-vivienda/)) towns like Cotacachi, Quiroga, and Imantag have  
43 developed on top of these deposits without considering the hazards related to living  
44 close to a potentially active volcano.

45 Over the last decades, large explosive eruptions have occurred worldwide (e.g.,  
46 Chaitén 2008, Lara et al., 2009; El Reventador 2002, Hall et al., 2004; Mt. Pinatubo  
47 1991, Newhall and Punongbayan, 1996; among others) highlighting the importance  
48 of understanding the eruptive chronology of poorly known volcanic centres or  
49 complexes such as Cotacachi-Cuicocha; especially if they have displayed highly  
50 explosive activity in the past and are in close proximity to a large population.

51 During the past thirty years, the IG-EPN (Instituto Geofísico, Escuela Politécnica  
52 Nacional, Ecuador) and the IRD (Institut de Recherche pour le Développement,  
53 France) have conducted several studies intended to reconstruct the eruptive  
54 chronology of the main Ecuadorian volcanic centres, such as Chachimbiro (Bernard  
55 et al., 2014), Cayambe (Samaniego et al., 1998; Samaniego et al., 2005), Imbabura  
56 (Le Pennec et al., 2011; Andrade et al., 2019), Cotopaxi (Hall and Mothes, 2008),  
57 Antisana (Hall et al., 2017), Pichincha (Robin et al., 2010), Pululahua (Andrade et  
58 al., 2021; Vásconez Müller et al., 2022), Atacazo-Ninahuilca (Hidalgo et al., 2008),  
59 Tungurahua (Hall et al., 1999; Bablon et al., 2018), Chimborazo (Samaniego et al.,  
60 2012), Carihuairazo (Samaniego et al., 2022), Sangay (Monzier et al., 1999,  
61 Valverde et al., 2021), and others along the Ecuadorian Volcanic Arc (Bablon et al.,  
62 2020). These studies aim a better understanding of the development of the  
63 Ecuadorian arc volcanoes and strongly contribute to volcanic hazards assessment.

64 This work is part of this long-term program and aim to fill a gap concerning the  
65 Cotacachi-Cuicocha eruptive chronology.

66 Previous unpublished research has been mainly devoted to the Cuicocha caldera-  
67 forming eruption products (von Hillebrandt, 1989; Pidgen, 2014), and more recently  
68 to the current gas emissions observed in the caldera lake (Sierra et al., 2020; Melián  
69 et al., 2021). Indeed, Cuicocha volcano seismic and degassing activity is closely  
70 monitored by the Instituto Geofísico of the Escuela Politécnica Nacional University  
71 (IG-EPN) from Ecuador (Sierra et al., 2020). However, despite its proximity to  
72 densely populated areas, the eruptive history of the CCVC remains poorly  
73 documented. The purpose of this work is to provide a first geological map of the  
74 whole volcanic complex to address the lack of knowledge about the evolution of  
75 CCVC, based on new chronological, petrographic, and chemical data collection.

76

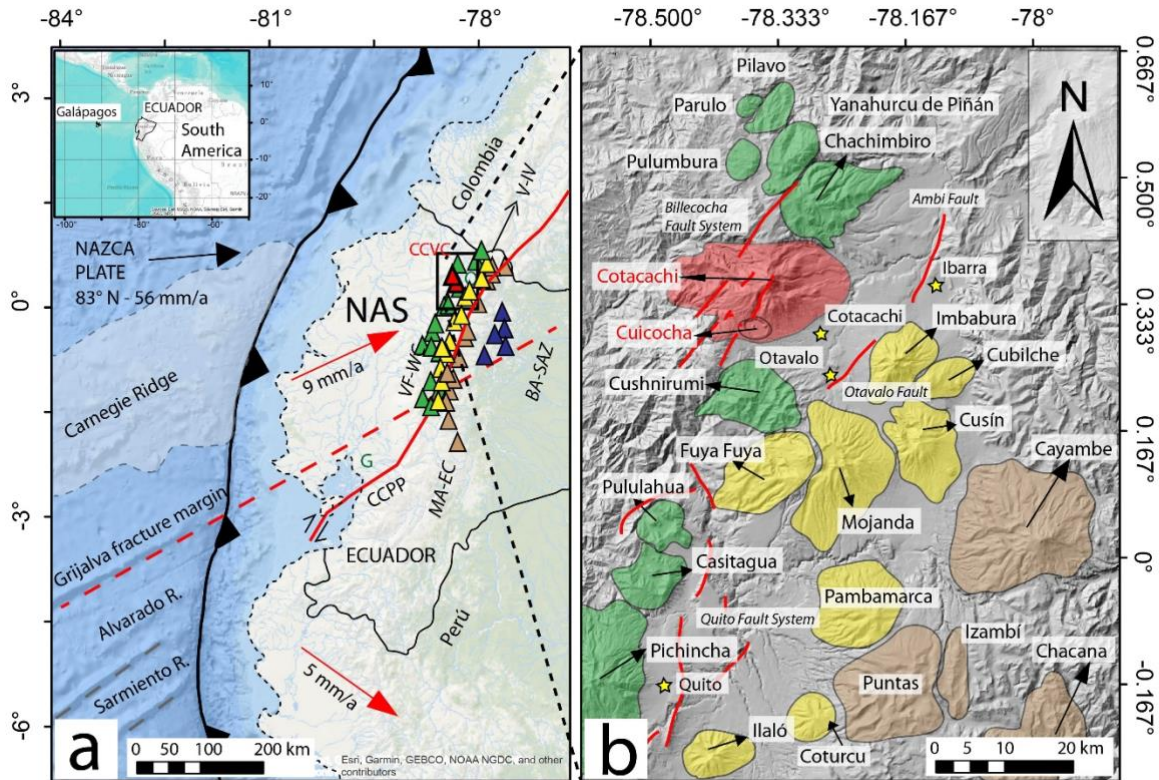
## 77 **2. GEOLOGICAL CONTEXT**

### 78 **2.1. Geodynamical and geological context**

79 The Ecuadorian volcanic arc results from the subduction of the oceanic Nazca plate  
80 beneath the South American continental plate (Hall and Wood, 1985; Barberi et al.,  
81 1988), with a convergence rate of  $56 \text{ mm.yr}^{-1}$  (relative to the stable Brazilian shield;  
82 Trenkamp et al., 2002; Nocquet et al., 2014; Fig. 1). As a result, the Ecuadorian Arc  
83 is divided into four north-south volcanic alignments, which are located along the main  
84 morpho-structural domains (i.e., Western Cordillera, Inter-Andean Valley, Eastern  
85 Cordillera, and the sub-Andean zone; Hall et al., 2008). The CCVC is constructed  
86 on the Western Cordillera basement, a Late Cretaceous mafic volcanic complex  
87 (Pallatanga and Río Cala units; Fig. 2) and related sedimentary rocks (Natividad  
88 Unit; Fig. 2). These basement is interpreted as a part of the Caribbean-Colombian  
89 Oceanic Plateau with overlapping deposits of an intra-oceanic magmatic arc  
90 sequence, accreted to the continental margin during the Late Cretaceous (Goosens  
91 and Rose, 1973; Feininger and Bristow, 1980; Hughes and Pilatasig, 2002; Kerr et  
92 al., 2002; Jaillard et al., 2004; Pratt et al., 2005; Spikings et al., 2005; Luzieux et al.,  
93 2006, Vallejo et al., 2006, Vallejo et al., 2009, Vallejo et al., 2019). These mafic  
94 terrains also present quartz-diorite intrusions such as the Apuela batholith, dated at

95 16.5 ± 1.1 Ma (van Thournout, 1992; Boland et al., 2000. Fig. 2). Finally, the Late  
 96 Oligocene – Early Miocene Silante formation (Vallejo et al., 2020) closes off the  
 97 basement sequence bellow Cotacachi and consists of a succession of continental  
 98 volcanoclastic sediments (Hughes and Bermudez, 1997; van Thournout, 1992;  
 99 Boland et al., 2000).

100



101

102 *Figure 1. a) Geodynamic context of the Ecuadorian volcanic arc (modified from Yepes et al., 2016)*  
 103 *and the spatial location of the four volcanic alignments (Bernard and Andrade, 2011; Hall et al., 2008).*  
 104 *VF-WC: volcanic front of the Western Cordillera (green, red triangles for Cotacachi and Cuicocha*  
 105 *volcanoes), V-IV: volcanoes of the Inter-Andean Valley (yellow), MA-EC: the main arc of the Eastern*  
 106 *Cordillera (brown), and BA-SAZ: the rear arc of the Sub-Andean zone (blue). The main morpho-*  
 107 *tectonic structures are NAS (North Andean Sliver), CCPP (fault system of Chingual-Cosanga-*  
 108 *Pallatanga-Puná), and the Billecocha, Huayrapungo and Quito fault systems (Ego et al., 1996; Eguez*  
 109 *et al., 2003; Jomard et al., 2021), and Río Ambi and Otavalo faults (Alvarado et al., 2016; Andrade*  
 110 *et al., 2019); G: City of Guayaquil. b) Close-up view of the CCVC area, with the different volcanic*  
 111 *systems colored as in a). Active faults from the Billecocha Fault System are shown with red lines, and*  
 112 *cities are located with a yellow star.*

113

114 **2.2. Neotectonic context: the Billecocha Fault System (BFS)**

115 The Billecocha Fault System (BFS. Ego et al., 1996; Eguez et al., 2003; Jomard et  
116 al., 2021; Figs. 1 and 2) appears as an eroded plateau-like morphology over the  
117 moorlands north of Cotacachi volcano (Fig. 3a), close to Cristococha Lake (Fig. 2  
118 and 3b). The present morphology of the moorlands is related to the last glaciation  
119 (ca. 14 - 33 ka; Clapperton, 1990) and subsequent levelling out by the deposition of  
120 volcanic deposits during the Holocene (Ego, 1996). The Billecocha Plateau and its  
121 surrounding volcanoes are heavily affected by active faulting characterized by  
122 straight, sharp, and discontinuous scarps (Jomard et al., 2021). These structures  
123 possibly accommodate the convergence stresses of the Nazca plate subduction  
124 beneath South America through the suture planes of the Cretaceous-Eocene  
125 accretions (Boland et al., 2000; Hughes and Pilatasig, 2002). In this context, the BFS  
126 could correspond to a surface expression of a tectonic reactivation of the Pujilí  
127 Suture (Baize et al., 2020; Jomard et al., 2021). The slip rate of Billecocha was  
128 constrained at around 2 mm/yr (Ego et al., 1996; Eguez et al., 2003). Despite being  
129 located within the North Andean Sliver (NAS), the Billecocha Fault System has no  
130 direct relation to neither the NAS stress regime nor to the Chingual-Cosanga-  
131 Pallatanga-Puná (CCPP; Fig. 1) fault system (slip rate of 8-10 mm/yr; Nocquet et al.,  
132 2014; Alvarado et al., 2016). The approximate length of the Billecocha fault system  
133 is 6-7 km, striking approximately north 25° and dipping to the south-east (Eguez et  
134 al., 2003). This structure has also been considered as a normal fault due to the  
135 presence of scarps, sag-ponds, and drainage cuts (Ego et al., 1996; Eguez et al.,  
136 2003). The morphology of the fault scarp and some detailed studies of kinematics  
137 and chronology in the associated stratigraphy suggest that its last movement  
138 occurred between 5.7 and 10 ka (Ego et al., 1996, Eguez et al., 2003). This  
139 assumption was corroborated by Jomard et al. (2021), who mention that the current  
140 activity of this fault system is low.

141

### 142 **3. ANALYTICAL METHODS**

143 Several field campaigns resulted in the detailed study of 79 outcrops (Appendix table  
144 A and appendix figure A.1) related to the Cotacachi-Cuicocha Volcanic Complex.  
145 Fieldwork included geological mapping (1:25.000 scale) and sampling of the

146 principal stratigraphic units, resulting in a collection of 52 unaltered samples for  
147 geochronological, petrographic, and geochemical analyses.

148

### 149 **3.1. Geochronology**

150 Considering the volcano stratigraphy, as well as the sample freshness and their low  
151 vesicularity, we selected 9 lava samples and one juvenile block from a block-and-  
152 ash-flow deposit. These samples were dated using the potassium-argon (K-Ar)  
153 method (Table. 1a) with the unspiked Cassinol-Gillot technique (Cassinol and  
154 Gillot, 1982; Gillot et al., 2006), which was shown to be suitable for calc-alkaline  
155 samples from Quaternary arc volcanoes (e.g., Germa et al., 2011; Ricci et al., 2015;  
156 Bablon et al., 2018). This technique determines the radiogenic argon ( $^{40}\text{Ar}^*$ ) content  
157 of the sample and compares the  $^{40}\text{Ar}/^{36}\text{Ar}$  ratios of both the sample and the  
158 atmosphere measured in the same condition. Since the groundmass of a lava flow  
159 is the last phase to crystallize when it cools after being erupted, its initial  $^{40}\text{Ar}/^{36}\text{Ar}$   
160 ratio corresponds to that of the atmosphere (*i.e.*, it does not contain any excess  
161  $^{40}\text{Ar}^*$ ). On the contrary, phenocrysts such as plagioclase or biotite can carry inherited  
162  $^{40}\text{Ar}$  that could significantly bias ages towards older values (e.g., Harford et al., 2002;  
163 Samper et al., 2008). Therefore, we carried out our measurements on groundmass,  
164 after removing phenocrysts using heavy liquids and magnetic separations. One  
165 measurement was carried out on separated plagioclase crystals to compare the  
166 result with the age obtained on groundmass. Details of analytical procedures, decay  
167 constants, standards used, and uncertainty calculations are given in Bablon et al.  
168 (2018). Both potassium and argon measurements were carried out at the GEOPS  
169 laboratory at Orsay (Paris-Saclay University, France) using an Agilent 240 Series  
170 AA flame absorption spectrometer and a multi-collector  $180^\circ$  sector mass  
171 spectrometer, respectively. Measurements were performed at least twice to check  
172 their reproducibility within their uncertainty range, at the  $1\sigma$  level. Final ages and  
173 uncertainties were calculated by averaging each analysis, weighted by their  $^{40}\text{Ar}^*$   
174 content.

175 The age of Cuicocha caldera explosive sequence was constrained by five new  
176 radiocarbon ages obtained from charcoal and soil samples collected from pyroclastic

177 deposits. These samples were analysed at the Center for Isotope Research (CIO),  
178 Groningen University (The Netherlands). Table 1b compiles the sample chronology  
179 with conventional  $^{14}\text{C}$  ages ( $\pm 1\sigma$ ) as well as calibrated ages ( $\pm 1\sigma$  and  $2\sigma$ ).  
180 Conversion from conventional  $^{14}\text{C}$  ages to standard and calendar ages was carried  
181 out using the Calib 7.1 code (Stuiver and Reimer, 1993; Stuiver et al., 2005) and the  
182 Northern Hemisphere calibration curve (IntCal20, Reimer et al., 2020).

183

### 184 **3.2. Petrography and geochemistry**

185 Thin sections of 52 samples were used to establish the samples petrography (modal  
186 counting, texture, and structures) using a petrographic microscope (ZEISS AXIO  
187 Scope A1; Appendix table B.1). Whole-rock chemical analyses of major and trace  
188 elements for 61 samples spanning the entire volcanic history were carried out at the  
189 Laboratoire Geo-Ocean (IUEM-UBO, Brest, France; Appendix table B.2).  
190 Measurements were performed on agate-crushed powders by ICP-AES (Inductively  
191 Coupled Plasma – Atomic Emission Spectroscopy). The relative standard deviation  
192 is 1% for  $\text{SiO}_2$  and 2% for the other major elements, except for low concentrations  
193 ( $<0.50\%$ ) for which the absolute standard deviation is 0.01%. The analytical  
194 procedure is described in Cotten et al. (1995).

195

### 196 **3.3. Edifice volume, construction and erosion rates estimates.**

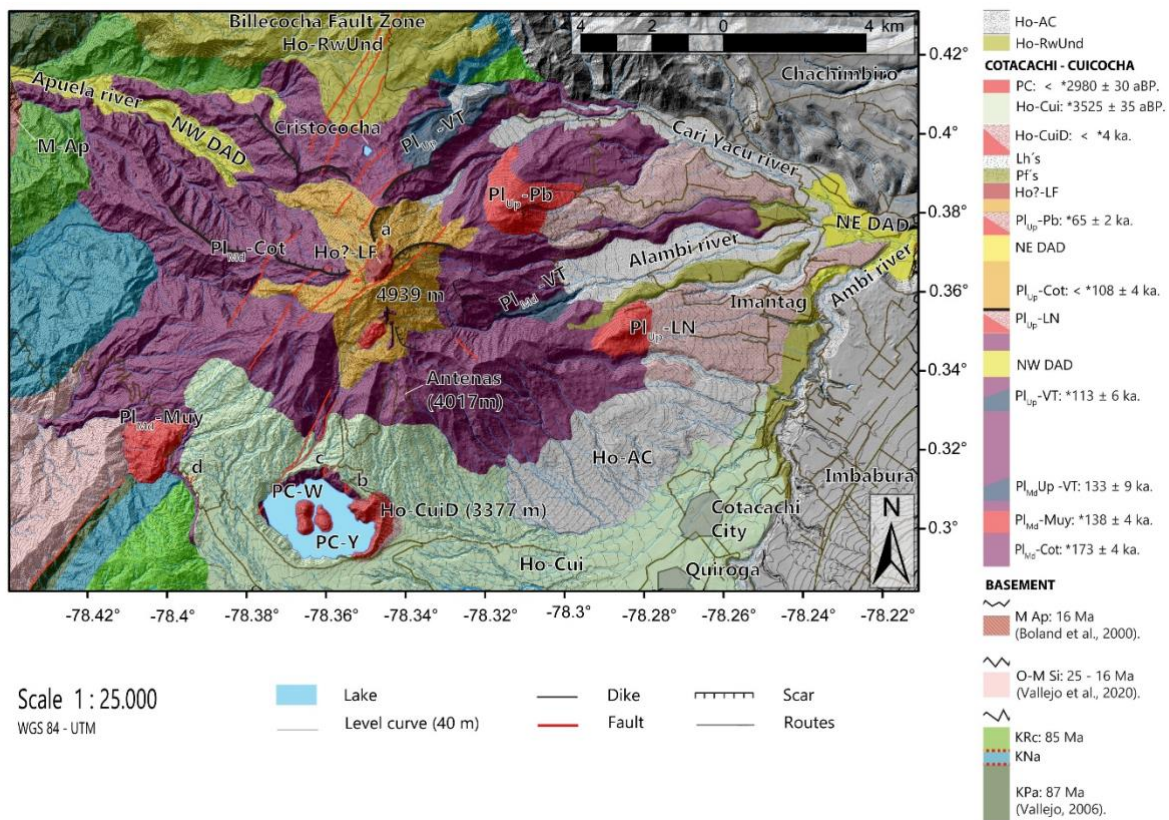
197 To quantify the morphological characteristics of this volcanic complex, we used two  
198 digital elevation models (DEM), one developed by the Instituto Geográfico Militar  
199 (IGM) of 30-m resolution, and a second model of 4-m resolution from SIGTIERRAS  
200 project, by the Ministry of Agriculture and Livestock  
201 (<https://www.agricultura.gob.ec/sigtierras/>). In this study, we used the 30-m for  
202 regional (e.g., for traces of regional fault systems and description of the morphology  
203 of stratigraphic units) and the 4-m one for local analyses (e.g., identification of small  
204 volcanic structures as land-scarps, estimation of slopes and volume calculations).  
205 Quantification of the minimum edifice volume, reconstruction, and erosion rate  
206 estimates were performed in two different ways: The first method for volume



207 estimation considers linear interpolation using a MATLAB® script, which applies the  
 208 volcano's baseline to create an interpolated grid that depicts the underlying  
 209 basement (Table 2a). This method does neither consider those parts underneath the  
 210 observed base nor those that were already eroded (see Andrade et al., 2021). In  
 211 contrast, the second method, developed by Lahitte et al. (2012), and further  
 212 improved by Germa et al. (2015), uses the ShapeVolc algorithm and ArcGis software  
 213 to make numerical surface interpolations based on the present-day topography of  
 214 the basement and the CCVC's crest elevations (Table 2b). It consists of numerical  
 215 modelling of the pre-erosional shape of the volcano, based on the extrapolation of  
 216 the uneroded surfaces such as crests (Dibacto et al., 2020).

217  
 218  
 219

#### 4. RESULTS



220

221 *Figure 2. Geological map of the Cotacachi-Cuicocha volcanic complex. Ho-AC: Alluvial and colluvial*  
 222 *deposits. Ho-RwUnd: Undifferentiated, reworked volcanoclastic deposits. PC: Post-caldera Domes*  
 223 *(W: Wolf, Y: Yerovi). Ho-Cui: Cuicocha pyroclastic density currents. Ho-CuiD: Cuicocha pre-caldera*  
 224 */ block and ash deposits. HO? -LF: Lava flows of the summit. Lh's: Lahar deposits of Cotacachi. Pf's:*  
 225 *Pyroclastic deposits of Cotacachi. Summit lava flows. PIUp-Pb: Piribuela dome / block and ash*

226 *deposits. NE DAD: Northeastern debris avalanche deposit. PIUp-LN: Loma Negra dome / block and*  
227 *ash deposits. PIUp-Cot: Upper Cotacachi Member. NW DAD: Northwestern debris avalanche deposit.*  
228 *PIMd-Up-VT: Verde Tola Unit. PIMd-Muy: Muyurcu dome. PIMd-Cot: Basal Cotacachi Member.*  
229 *MioAp: Apuela batholith. EOSi: Silante Unit. KRc: Río Cala Unit. KNa: Natividad Unit. KPa: Pallatanga*  
230 *Unit. Letters: a, b, c and d are related to the locations of figure 5 outcrops of neotectonics. \* For the*  
231 *new ages obtained during this study.*

232

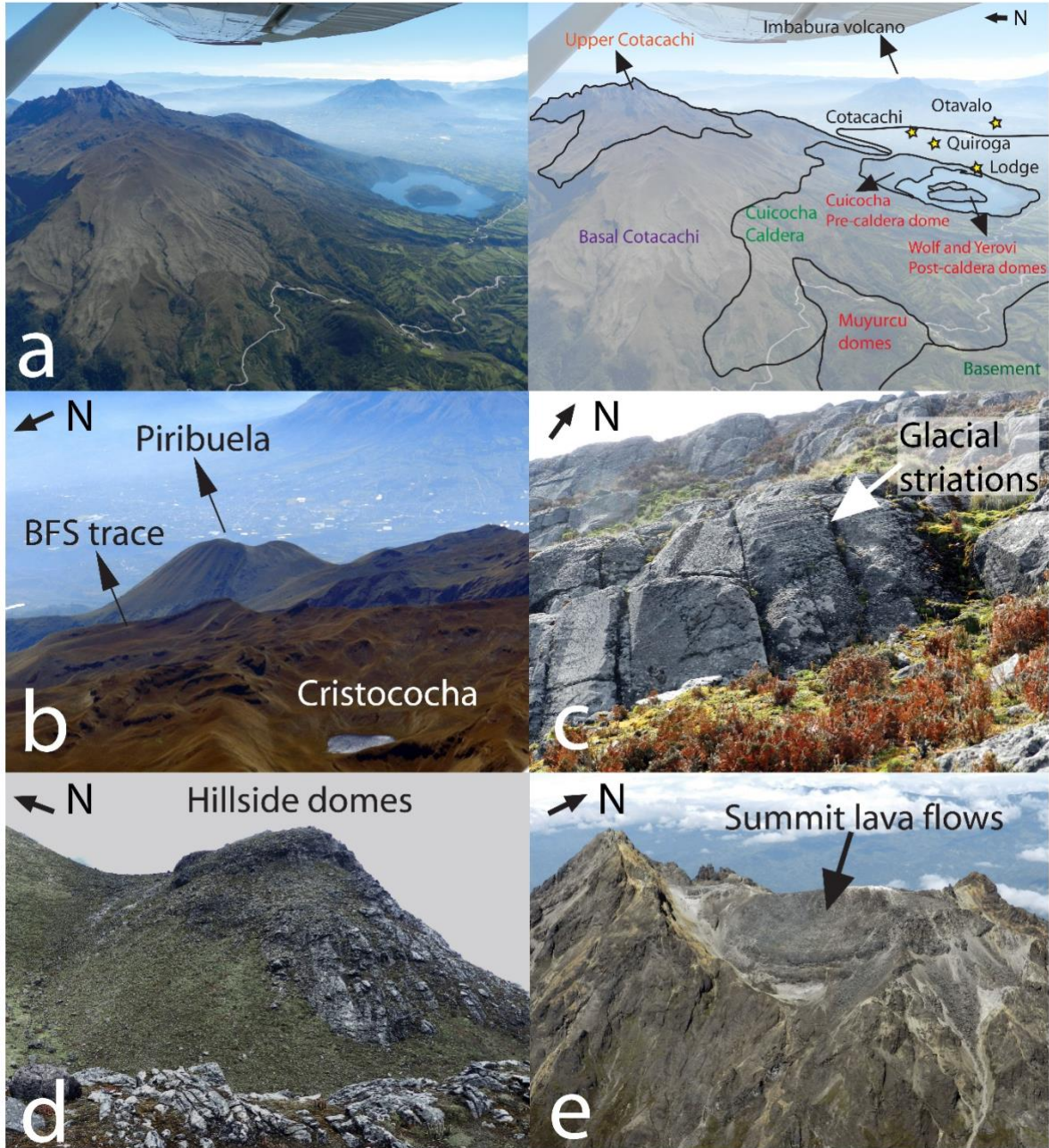
#### 233 **4.1. Morphology and structure of CCVC**

234 The Cotacachi composite stratovolcano is the main edifice of the Cotacachi-  
235 Cuicocha volcanic complex. Its basal surface covers an area of ~268 km<sup>2</sup>, with a  
236 north-south axis of 14-15 km and an east-west axis of 20-21 km (Figs. 2, 3).  
237 Cotacachi volcano lower flanks are characterized by smooth slopes (6° - 25°;  
238 Appendix figure A.2) and radial U-shaped glacial valleys, especially at the southern  
239 and eastern flanks, which are partially filled with moraine deposits as well as local  
240 and regional pyroclastic deposits. The moraines are in the high moorlands (between  
241 3700 to 3800 m above sea level - asl) north of the edifice and are mostly visible  
242 around a small glacial lake called Cristococha (3777 m asl; Fig. 3b). The presence  
243 of radially oriented, deep glacial valleys, the frequent glacial striations displayed by  
244 basal lavas (Fig. 3c), and the associated moraines, have been attributed to the Late  
245 Pleistocene glaciations (Last Glacial Maximum - LGM), dated in the range of ca. 33  
246 to 14 ka (Clapperton, 1990; Samaniego et al., 2012; Bablon et al., 2019) in this part  
247 of the Andes. Towards the top of the edifice, the upper Cotacachi flanks (Fig. 3a) are  
248 characterized by an abrupt change of slope (17° – 35°, Appendix figure A.2),  
249 sculpting a pyramidal structure strongly affected by glacial erosion processes.  
250 Indeed, the presence of smaller, young-looking moraines, reaching down to 3700 m  
251 asl suggests that the terminal Cotacachi edifice was also affected by the glacial  
252 advances younger than the LGM (i.e., the Younger Dryas and/or the Neoglacial  
253 event, roughly dated at 10-12 ka and ~5 ka respectively; Clapperton, 1990). The  
254 remnants of the last glaciers on the northern and eastern flanks of the volcano were  
255 reported by Whymper (1892), Wolf (1892), and Troya (1913). Towards Cotacachi  
256 volcano summit, on its southern flank, behind some relatively small hillside domes  
257 (Fig. 3d), two major peaks (4939 m asl and 4756 m asl, respectively) aligned north-

258 south stand out. These peaks delimit a crater, inside which a dome-like structure  
259 characterized by the absence of glacial erosion is observed (Fig. 3e).

260 Two groups of medium- to large-size scars of deep horse-shoe shaped depressions  
261 are present on the north-western and north-eastern flanks of Cotacachi (3 to 10 km  
262 wide; Appendix figure B). One is open towards the NW with a maximum width of 5-  
263 6 km, while the second open towards the NE with an opening of 6-7 km. The lava  
264 flows that constitute the main cone-building stage crop out at the inner walls of  
265 escarpments. Additionally, younger, and smaller (2-3 km, Appendix figure B, black  
266 coloured scars) scars were observed inside the largest one (Appendix figure B, blue  
267 coloured scars) and may correspond to landslides produced by gravitational  
268 processes or perhaps recent seismic activity (e.g., 7.0 – 7.3 M August 16<sup>th</sup>, 1868 -  
269 Ibarra earthquake, Beauval et al., 2010; Madera, 1918).

270



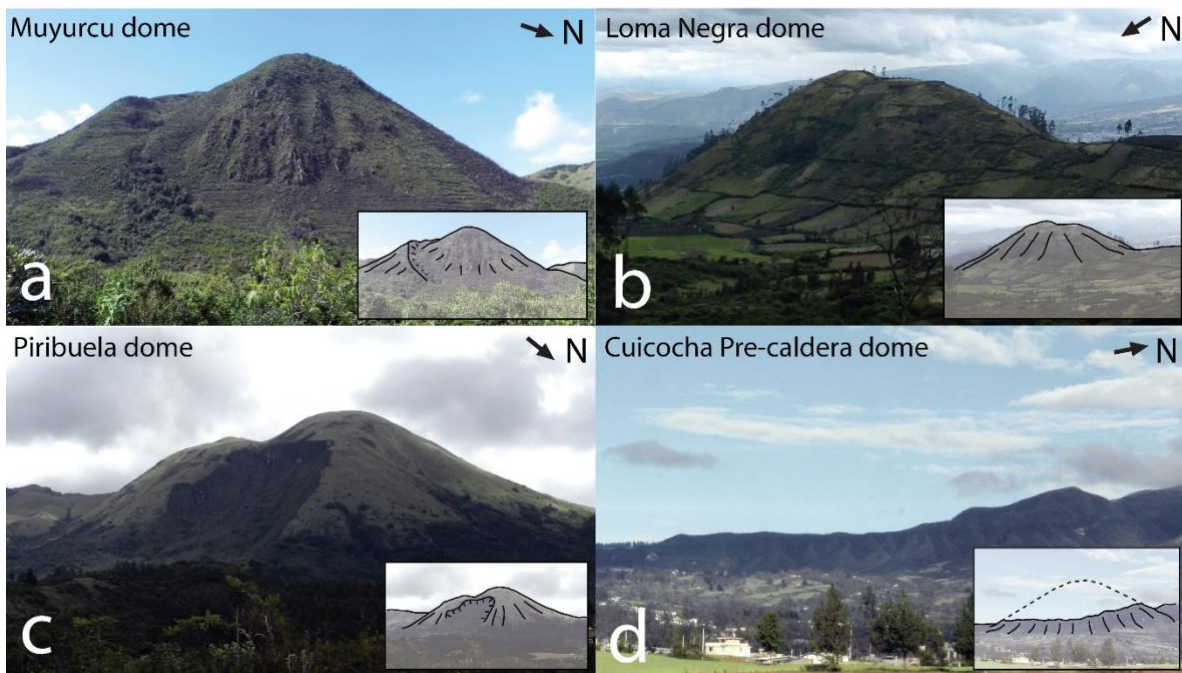
271

272 *Figure 3. a) Aerial photograph and illustration of the different stratigraphic members of the Cotacachi-*  
 273 *Cuicocha volcanic complex. The yellow stars represent the populations closest to the volcanoes. b) Cristococha*  
 274 *(0.396° N; 78.349° W) post-glacial lake and the different associated moraine deposits*  
 275 *(between 3600 to 3900 m asl, on the north-western flanks of Cotacachi). c) Sub-horizontal glacial*  
 276 *striated lava flows (0.350° N; 78.345° W) corresponding to basal Cotacachi (between 3450 to 4000 m*  
 277 *asl, on the southern flank). d) Viscous lava flows (0.352° N; 78.346° W) forming a lava dome on the*  
 278 *hillside southern flank of the volcano. e) Aerial photograph of the amphitheater of the Cotacachi*  
 279 *volcano crater. Note the unglaciated summit lava flows (0.367° N; 78.346° W) or domes*  
 280 *superimposed horizontally inside the crater.*

281

282 Moreover, several volcanic domes are distributed around the Basal Cotacachi edifice  
 283 (Figs. 2, 4). Some of them are observed as compound domes (Muyurcu: 3502 m asl;  
 284 Fig. 4a), and others as dome clusters (Loma Negra: 3066 m, Fig. 4b; Piribuela: 3871  
 285 m asl, Fig. 4c). In addition, the remnants of the Cuicocha pre-caldera dome (3377 m  
 286 asl; Fig. 4d) are observed west of Cuicocha caldera (Fig. 2), which has an elliptical  
 287 shape and reaches 3.2 km from east to west and 2.3 km from north to south. The  
 288 caldera rim is limited by steep walls (55 to 90°, 5.1 km<sup>2</sup>; Appendix figure A.2) which  
 289 have been filled by almost 0.3 km<sup>3</sup> of a meteoric water lake, occupying a minimum  
 290 area of 3-4 km<sup>2</sup> (Gunkel and Beulker, 2009). The maximum water depth is 148 m,  
 291 with a mean depth of 72 m (Gunkel and Beulker, 2009). Two east-west aligned islets  
 292 located in the centre of the caldera lake correspond to post-caldera domes (Fig. 2).  
 293 These islets are named Wolf (3247 m asl) and Yerovi (3142 m asl) and cover 0.5  
 294 and 0.3 km<sup>2</sup> of the lake surface, respectively.

295



296

297 *Figure 4. Photographs of the peripheral domes of Cotacachi volcano (see Fig. 2 for geographic*  
 298 *location). In chronological order: a) Muyurcu dome (0.323° N; 78.398° W), b) Loma Negra dome*  
 299 *(0.351°N; 78.284° W), c) Piribuela dome (0.383° N; 78.314° W), and d) Cuicocha dome amphitheater*  
 300 *(0.307° N; 78.348° W), observed from the east at the Selva Alegre – Quiroga road. Morphological*  
 301 *features, as well as possible reconstruction of the Cuicocha dome and the scarp over the south-*  
 302 *eastern flank of the Piribuela dome are shown as inserts at the bottom right.*

303

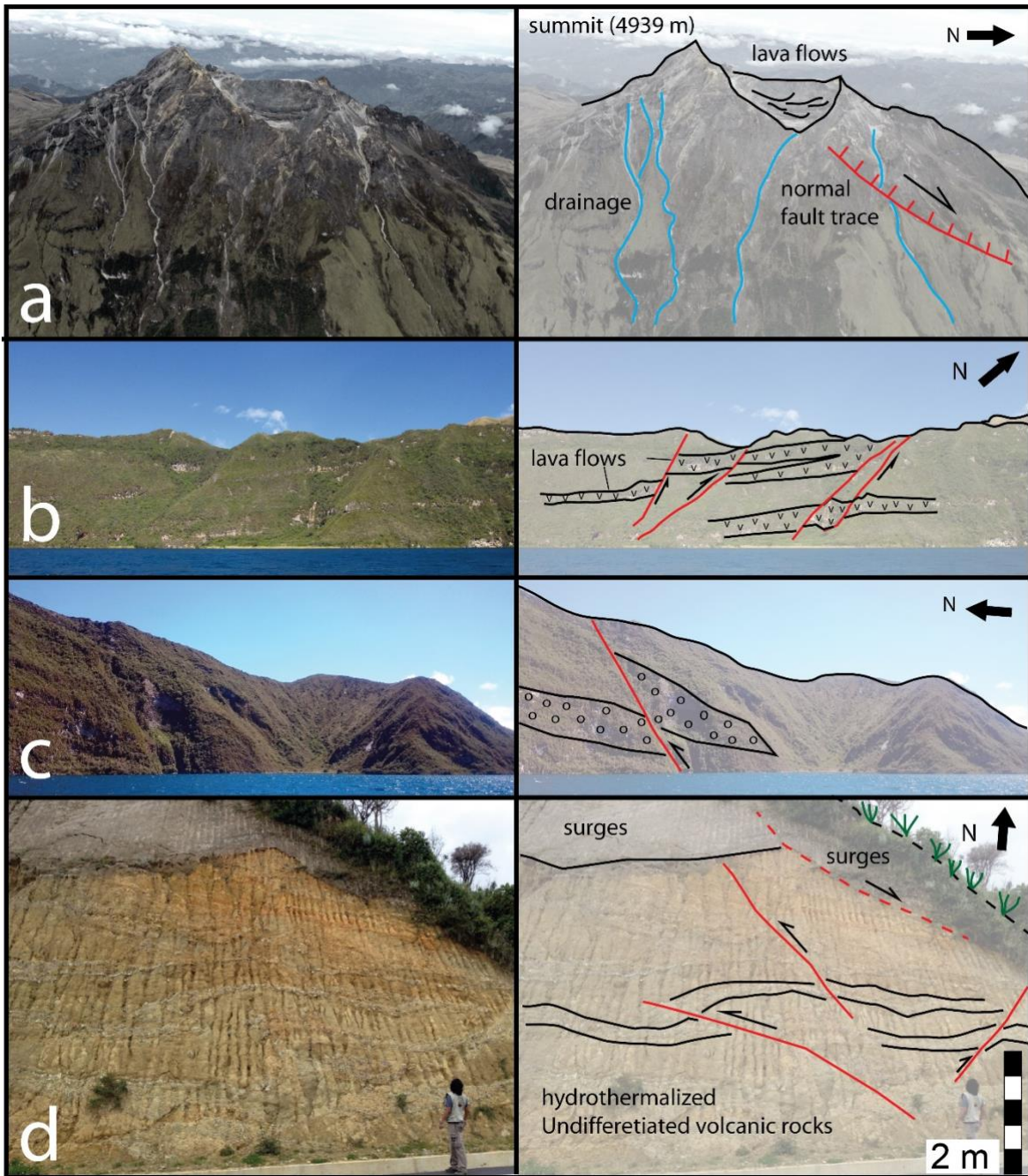
304

## 4.2. Main neo-tectonic structures of CCVC

305 Regional neo-tectonic structures of the Northern Andes cut across Cotacachi  
306 composite volcano (Fig. 5a). Lineaments along with rupture zones crop out at the  
307 western and northern walls of the Cuicocha caldera (Fig. 5b, 5c), extending across  
308 Cotacachi from the southwest to the northeast (N22°E, N45°E - dipping 30 to 35° N-  
309 NE). Displacements show apparent gravitational/extensional movements of the  
310 basal Cotacachi lavas. The lineaments and their associated fault kinematics were  
311 observed as trans-tensional/negative flower structure, and strike-slip faults with  
312 secondary normal components (Ego, 1996, Eguez et al., 2003, this study). Finally,  
313 the trace of the surface morphology looks like a horsetail structure (Fig. 2, Appendix  
314 figure B).

315 Outcrops along the Cuicocha – Apuela road, exhibit small faults with positive flower  
316 structures (Fig. 5d) with mostly compressive kinematics accompanied by some  
317 secondary gravitational structures, whose azimuth strikes similar to the NE – SW  
318 main Andean trend (Trenkamp et al., 2002; Eguez et al., 2003; Bourgois, 2013;  
319 Alvarado et al., 2016; Yepes et al., 2016). At this locality the faults propagate through  
320 the surge succession of Cuicocha caldera, a basal hydrothermally altered rock  
321 sequence, and the older Cotacachi lava flows.

322



323

324 Figure 5. Photographs of the different fault outcrops in the CCVC. The photographs and diagrams in  
 325 two dimensions are shown according to the potential size of the structure: a) prolongation of the  
 326 Billecocha fault system over the eastern flank ( $0.365^{\circ}$  N;  $78.339^{\circ}$  W) of Cotacachi volcano edifice.  
 327 The structure is observed as a normal type of fault with western vergence. The lava flows of the  
 328 summit are not affected. b) northwestern wall ( $0.311^{\circ}$  N;  $78.373^{\circ}$  W) of Cuicocha caldera lake,  
 329 different structures of negative flower type are observed. c) northern wall ( $0.311^{\circ}$  N;  $78.354^{\circ}$  W) of  
 330 Cuicocha caldera lake, a potentially inverse structure is observed. d) structures of positive flower type  
 331 ( $0.311^{\circ}$  N;  $78.394^{\circ}$  W) in the Holocene deposits of Cuicocha, at the base of the surges some hydro-  
 332 thermally altered and undifferentiated volcaniclastic deposits are observed.

333

334        **4.3.        Chronology of the CCVC**

335        ***Cotacachi Basal member***

336        *Main basal lava flows (PI<sub>Ma</sub>-Cot)*

337        Basal Cotacachi lava flows (purple unit in Fig. 2) are a monotonous, ~500 m-thick  
338        succession of sub-horizontal lava flows (Appendices figures C.1 and C.2), that reach  
339        up to 5-7 km from the summit. The most representative outcrops are located at the  
340        north-eastern and the south-western flanks of the volcano, between 2700 and 3900  
341        m asl, as well as at the inner northern walls of the Cuicocha caldera. This succession  
342        rests discordantly on the Cretaceous-Paleogene volcanic basement, covering a  
343        surface of 107 km<sup>2</sup>. Well-compacted matrix-supported breccias (30 vol.% of  
344        andesitic lithics) are interlayered between the lava flows. The lavas are porphyritic  
345        basaltic andesites and andesites (54.7 – 61.8 wt.% SiO<sub>2</sub>), with a mineral assemblage  
346        comprising plagioclase (11 vol. %), clinopyroxene (5 vol. %), orthopyroxene (3 vol.  
347        %), and olivine (2 vol. %) (e.g., COTA-08). K-Ar ages obtained from two samples  
348        taken near the base of the Cotacachi basal lava flows yielded ages of 173 ± 4 and  
349        163 ± 4 ka, respectively (COTA 54 and COTA-01, Table 1a and Appendix figure  
350        C.1). Three additional lava samples corresponding to the top of the basal lava flows  
351        yielded ages of 110 ± 6, 108 ± 6 and 108 ± 4 ka, respectively (COTA-05, CUI-28,  
352        and CUI-30A samples, Table 1a, Appendix figure C.1).

353

354

355

356

357

358

359

360

361



Sample	Lab Code	Location	Longitude (m)	Latitude (m)	Member, Unit	Phase	K (%)	<sup>40</sup> Ar <sup>+</sup> (%)	<sup>40</sup> Ar <sup>+</sup> x 10 <sup>11</sup> (at/g)	Age ± 1σ (ka)	Mean age (ka)	
a	COTA 54	17EQ86	Distal lava flow, SW flank	787198	10037876	Basal Cotacachi	Groundmass	1.510	4.72	2.6912	171 ± 4	173 ± 4
									6.07	2.7518	174 ± 4	
	COTA 01		Lava flow, E valley	798773	9838736	Basal Cotacachi	Groundmass	1.075	4.32	1.7989	160 ± 4	163 ± 4
									4.38	1.8683	166 ± 4	
	COTA 56	17EQ88	Muyurcu dome, SW flank	789687	10035549	Muyurcu dome	Groundmass	1.378	3.60	2.0004	139 ± 4	138 ± 4
									4.53	1.9669	137 ± 4	
	COTA 02		Lava flow, SE flank	800141	9839050	Verde Tola Unit	Groundmass	0.952	1.53	1.3566	136 ± 9	133 ± 9
									1.56	1.2926	130 ± 9	
	COTA 012		Proximal lava flow, S flank	795416	10038627	Upper Cotacachi	Groundmass	2.001	5.33	2.5751	123 ± 3	122 ± 8
									6.41	2.3856	114 ± 2	
									5.68	2.7248	130 ± 3	
	COTA 60	17EQ93	Distal lava flow, NE flank	797793	10045132	Verde Tola Unit	Groundmass	1.133	1.77	1.4370	121 ± 7	113 ± 6
									2.23	1.2733	108 ± 5	
	COTA 05		Lava flow, E flank	798715	9838058	Basal Cotacachi	Groundmass	1.175	2.12	1.3089	111 ± 5	110 ± 6
									2.13	1.3826	113 ± 6	
	CUI 28		Lava flow, S flank	796267	9836562	Basal Cotacachi	Groundmass	1.156	1.66	1.2859	107 ± 7	108 ± 6
								2.40	1.3150	109 ± 5		
CUI 30A		Lava flow, S flank	795354	9836039	Basal Cotacachi	Groundmass	1.522	2.68	1.7491	110 ± 4	108 ± 4	
								3.28	1.6799	106 ± 4		
								0.186	0.66	0.3353		173 ± 26
COTA 26		Block from a PF deposit, NE flank	801184	10041881	Piribuela Dome	Groundmass	2.529	0.97	0.4492	231 ± 24	207 ± 25	
								3.88	1.7183	65 ± 2		
COTA 57	17EQ89	Lava flow, Cuicocha dome	795129	10032404	Cuicocha	Groundmass	1.302	6.08	1.6972	64 ± 1	65 ± 2	
								< 0.1	-0.0092	< 4		

362

363

Sample	Lab code	Locality	Longitude (m)	Latitude (m)	Unit	Type of sample	<sup>14</sup> C age (years BP)	d <sup>13</sup> C (o/oo)	Calendar age range (2 sigma) - InCAL20 (cal BP)	Relative area (%)	Calendar age range (1 sigma) - InCAL20 (cal BP)	Relative area (%)
<b>b</b>	CUI-27C	GrA 54410	Organic soil under ash before surges	796378	10037549	Cuicocha	soil	5750 ± 35	-24.77	95	6449 - 6647	19
											6493 - 6565	50
	CUI-22A	GrA 54412	Soil under pyroclastic flow	790562	10034145	Cuicocha	soil	4470 ± 35	-23.01	95	4973 - 5290	4
											5041 - 5070	10
											5102 - 5135	12
											5167 - 5279	43
	CUI-27B	GrA 54408	Organic soil under surges	796378	10037549	Cuicocha	soil	3525 ± 35	-25.24	95	3895 - 3695	2
											3819 - 3849	19
	CUI-22B	GrA 54411	Pyroclastic flow and surges	790562	10034145	Cuicocha	charcoal	2980 ± 30	-26.00	92	3060 - 3249	46
											3301 - 3324	3
											3033 - 3040	1
	CUI-27A	GrA 54406	Soil under ash fall after Cuicocha	796378	10037549	Cuicocha	soil	2245 ± 30	-25.71	68	2295 - 2339	3
2152 - 2265											42	
											2232 - 2301	23

364

365 Table 1. a) Potassium-argon (K-Ar) ages obtained in this study (see text for details). Column headings indicate sample  
 366 name, lab code, outcrop location, member/unit, dated phase of the sample, potassium content in percent, radiogenic argon  
 367 content in percent and in atoms per gram, age obtained for each measurement, weighted mean age in ka, given with 1-σ

368 uncertainty. Measurements were carried out on groundmass for all samples, and on plagioclase crystals for CUI 30A sample.  
369 b) Radiocarbon ages obtained from charcoal and soil samples collected in pyroclastic deposits. <sup>14</sup>C chronology table gives  
370 the conventional ages ( $\pm 1\sigma$ ), and the calibrated ages ( $\pm 1\sigma$  and  $2\sigma$ ) to standard and calendar ages, using the Calib 7.1 code  
371 (Stuiver and Reimer, 1993; Stuiver et al., 2005) and the Northern Hemisphere calibration curve (IntCal13, Reimer et al.,  
372 2013; IntCal20, Reimer, 2020).

373 *Muyurcu domes unit (Pl<sub>Md</sub>-Muy)*

374 Muyurcu (3502 m asl) (Fig. 4a) is a small (1.5 - 2 km in diameter, with a surface of  
375 2.4 km<sup>2</sup>) compound dome, which is located at the lower south-western flank of  
376 Cotacachi (red unit in Fig. 2). Muyurcu dome is composed of a porphyritic, light grey-  
377 coloured andesite (60.2 – 61.7 wt.% SiO<sub>2</sub>) with plagioclase (13 vol. %), pyroxene (8  
378 vol. %), and rare amphibole phenocrysts (4 vol. %). A K-Ar age obtained from a lava  
379 sample from the summit (Loma de la Virgen) yielded an age of 138 ± 4 ka (COTA-  
380 56; Table 1a). Importantly, this age agrees with the stratigraphic position of this unit,  
381 which is almost contemporaneous with the main lava flow succession of Cotacachi  
382 volcano basal member.

383

384 *Verde Tola unit (Pl<sub>Up</sub>-VT & Pl<sub>Md</sub>-VT)*

385 The olivine-rich Verde Tola lava flow succession (dark blue unit in Fig. 2), that forms  
386 the Verde Tola hill at the lower north-eastern flank of Cotacachi, reaches between  
387 3400 and 3900 m asl. This unit comprises a <100 m-thick lava flow succession, with  
388 individual lava flows having a maximum runout of 2-3 km from the inferred emission  
389 centre. Another < 30 m-thick lava flow succession crops out at the south-eastern  
390 flank of the volcano, by the headwaters (3300 m asl) of the Alambi river valley (Fig.  
391 2), where they concordantly overlay the Cotacachi basal lava flows, and reach 3 km  
392 from the emission centre at the highest point of the Verde Tola hill. These lavas are  
393 porphyritic, olivine-bearing basaltic andesites (54.7 - 55.9 wt.% SiO<sub>2</sub>), with a mineral  
394 assemblage of plagioclase (9 vol. %), clinopyroxene (3 vol. %), orthopyroxene (3 vol.  
395 %), and olivine phenocrysts (4 vol. %). Two lava samples of the Verde Tola unit from  
396 the SE and NE flanks were dated at 133 ± 9 (COTA-02) and 113 ± 6 ka (COTA-60,  
397 Table 1a, Appendix figure C.1), respectively.

398

399 *Loma Negra dome unit (Pl<sub>Up</sub>-LN)*

400 Loma Negra (3066 m asl) (red unit in Fig. 2, Fig. 4b) is an eroded lava dome located  
401 at the eastern flank of Cotacachi volcano, with a basal surface of 1.9 km<sup>2</sup>. It is  
402 covered by a thick layer of reworked, well-compacted, black-coloured soil displaying  
403 angular andesitic lithics. Loma Negra is composed of a porphyritic, light grey-

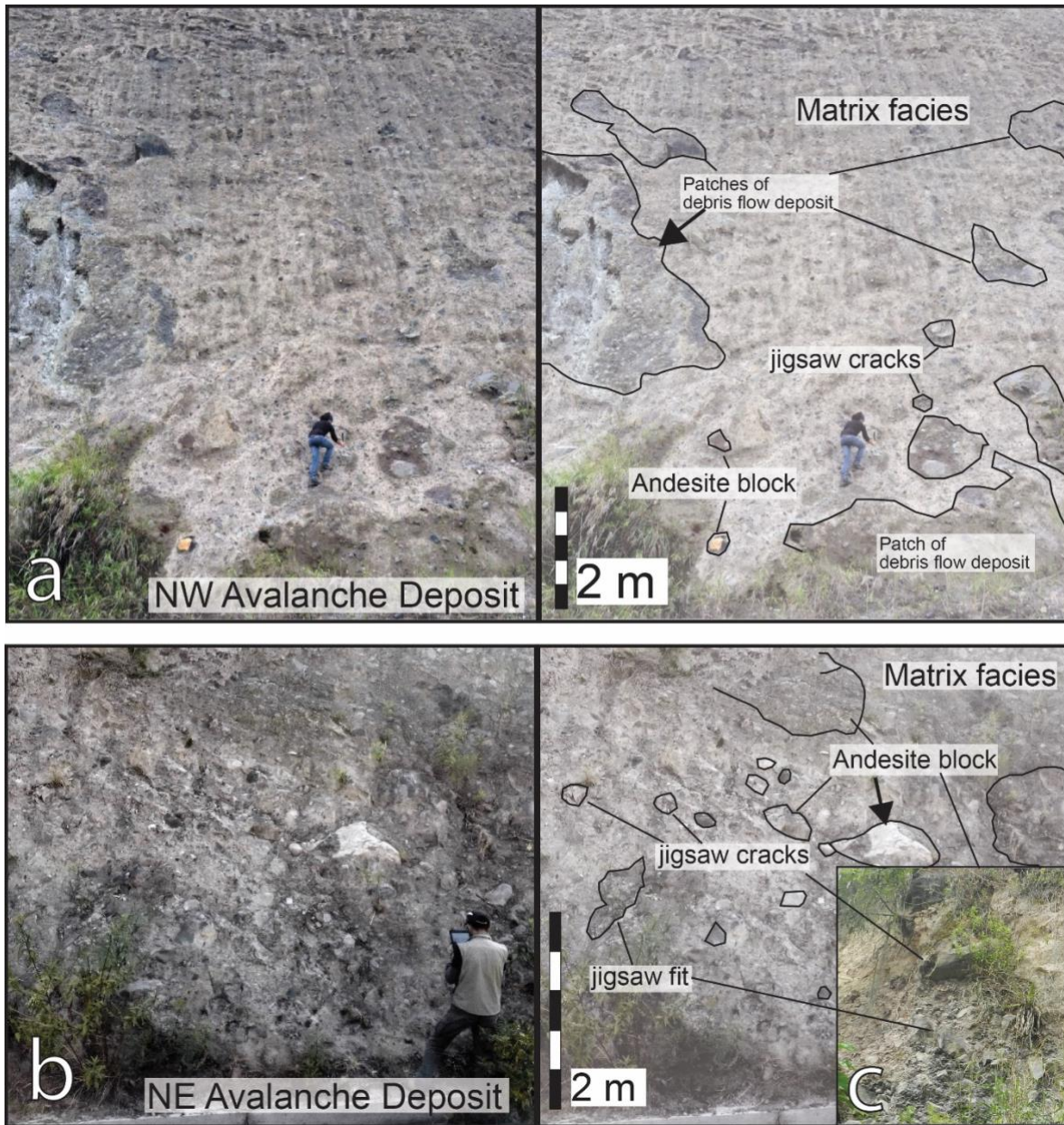
404 coloured andesite with plagioclase, amphibole, and scarce pyroxene phenocrysts.  
405 In addition, a matrix-supported mono-lithological breccia that includes the  
406 amphibole-bearing andesites (~20-30 vol.% of lithics) was identified at the eastern  
407 flank of Loma Negra dome (red hatched area in Fig. 2). This deposit has an  
408 estimated thickness of 10-20 m, reached 4-7 km from its inferred source, and covers  
409 a surface of 10-12 km<sup>2</sup>. Given its stratigraphic position cutting the Cotacachi lavas  
410 on the SE flank, this dome appears to be younger than the lava flows of the  
411 southeastern flank of Cotacachi, which were dated at ~110 ka.

412

#### 413 *Northwestern debris-avalanche deposit (NW DAD)*

414 This unit crops out 40 km along the Apuela river inside the Intag valley (yellow unit  
415 in Fig. 2), to the northwest and the southwest of the volcano. In the Intag valley, this  
416 deposit overlies part of the Western Cordillera basement formed by the Apuela  
417 quartz-diorite batholith (Boland et al., 2000). The NW-DAD has a maximum  
418 thickness of 60-70 m from the bottom of the river valley (COTA 40; at 35 km from  
419 the inferred source at north-western flanks of Cotacachi volcano, Appendix figure B)  
420 and forms conspicuous and isolated terraces along the valley (Fig. 6a, Appendix  
421 figure B). This deposit is a volcanic breccia characterized by blocky facies (approx.  
422 30 vol.% of the deposit, e.g., individual lithics of basaltic andesites, andesites, and  
423 some red and black volcanic scoria, as well as different patches of debris flow  
424 deposits) with variable diameters from 0.5 to 1 m (4 m for the debris flow deposit  
425 patches), embedded in a fine light-grey well-compacted matrix. The mineralogy of  
426 andesite lithics found within this deposit is characterized by the ubiquitous presence  
427 of pyroxene. Interestingly, no amphibole-bearing andesites were identified in the NW  
428 DAD. Dense volcanic blocks display frequent jigsaw fractures. Mixed facies are also  
429 present and constitute the main percentage (60 vol.%) of the distal avalanche  
430 deposit. The deposit displays fine matrix injections and other small subrounded  
431 lithics incorporated from the Western Cordillera basement, in addition to a small  
432 number of lithics from the Apuela quartz-diorite batholith (less than 10 vol.%, ~0.25  
433 m in diameter).

434



436

437 *Figure 6. Photographs of the (a) northwestern (Cota 40: 0.238046 N; 78.603827° W) and*  
 438 *northeastern (Cota 17: 0.398295° N; 78.135906° W) debris-avalanche deposits of the Cotacachi*  
 439 *volcano. The northwestern deposit is located at the road that leads to the Intag valley, close to the*  
 440 *Apuela town. The northeastern deposit is located at the Ambi river valley, close to the Imantag town.*  
 441 *An interpretation of the deposits and their main structures is shown to the right. (c) First plane picture*  
 442 *of the jigsaw – cracks and fit inside the NE avalanche deposit.*

443

444 ***Cotacachi Upper member***

445 *Upper lava flows (Pl<sub>Up</sub>-Cot)*

446 The upper member of the Cotacachi edifice (orange unit in Fig. 2) comprises a steep  
447 succession of lava flows (Figs. 3a and e). Access to these highly altered outcrops is  
448 very difficult, allowing only limited sampling of the southern flanks over 4000 m asl,  
449 on the ascent route to the summit. This lava flow succession reaches between 250  
450 and 350 m thickness with a 1-2 km runout from the summit. This unit covers a surface  
451 of 16 km<sup>2</sup> and includes some interlayered volcanic breccias. Also, the lava flows form  
452 an angular unconformity over the basal lava flow succession (Pl<sub>Mid</sub>-Cot). This unit is  
453 mainly formed by porphyritic andesites (59.8 – 60.7 wt.% SiO<sub>2</sub>), which include some  
454 andesitic enclaves. Some smaller (0.4 – 0.5 km<sup>2</sup>) viscous lava flows on the hillside  
455 (Fig. 3d) and summit (HO - LF; Fig. 3e) are part of this volcanic unit and are formed  
456 by siliceous andesites (61.9 – 62.3 wt.% SiO<sub>2</sub>) with a mineral assemblage of  
457 plagioclase (14 vol. %), orthopyroxene (2 vol. %), clinopyroxene (4 vol. %), and some  
458 scarce amphibole (2 vol. %) and olivine phenocrysts (< 1 vol. %). Sample COTA12  
459 taken from this unit yields an age of 122 ± 8 ka (Table 1a and Appendix figure C.1),  
460 which, within uncertainties, overlaps with the ages obtained from the top of the lava  
461 succession of Basal Cotacachi I (110 ± 6 to 108 ± 6 ka).

462

463 *Northeastern debris-avalanche deposit (NE-DAD)*

464 This unit crops out at 30 km from the Cotacachi volcano, forming the terraces of the  
465 Cari-Yacu and Ambi rivers (yellow unit in Fig. 2, Fig. 6b), along the north-eastern  
466 flank of the edifice. The NE-DAD appears beneath the Piribuela dome pyroclastic  
467 deposits (Appendices figures C.2 and B) and has a maximum thickness of 15-20 m  
468 (Cota 17, Cota 38). The NE-DAD is a consolidated volcanic breccia that includes  
469 block-rich facies (~25 vol.% of the deposit), which comprise debris flow deposit  
470 patches and large blocks of pyroxene-bearing andesites (typical of basal member),  
471 as well as a few amphibolic andesites and dacites (typical of the upper member).  
472 Some blocks (mainly andesites), from ~ 0.25 to 2 meters in diameter, showing  
473 frequent jigsaw fractures are also observed. This deposit has a fine-grained and  
474 cohesive matrix (75 vol.% of the deposit) and incorporated rounded basement lithics

475 (~ 0.5 m in diameter). The mineralogy and geochemistry of the lava blocks in this  
476 avalanche deposit suggest that this event affected both basal and upper members  
477 of the Cotacachi cone.

478 Given that lava samples from the overlying Piribuela domes (presented below) yield  
479 an age of  $65 \pm 2$  ka (Table 1a), and that the upper lava flows of the basal Cotacachi  
480 yielded ages of  $108 \pm 6$  and  $108 \pm 4$  ka (Table 1a), we propose that this debris-  
481 avalanche occurred between  $108 \pm 6$  and  $65 \pm 2$  ka. These ages agree with field  
482 observations, that the NE-DAD is distributed across the Ambi river valley, which was  
483 carved into the older Chachimbiro debris-avalanche deposit (dated between  $405 \pm$   
484  $20$  and  $298 \pm 32$  ka; Bellver-Baca et al., 2019). In addition, long the right bank of  
485 Ambi river, the NE-DAD is overlain by the Imbabura debris-avalanche deposit  
486 (whose age is bracketed between  $47 \pm 6$  and  $30 \pm 4$  ka; Le Pennec et al., 2011;  
487 Andrade et al., 2019; Appendix figure C.2).

488

#### 489 *Piribuela dome (Pl<sub>Up</sub>-Pb)*

490 Piribuela dome (3871 m asl, 3.6 km<sup>2</sup>) is located northeast of the Cotacachi summit  
491 volcano (red unit in Fig. 2, Fig. 4c). It is composed of porphyritic light grey and red-  
492 coloured dacites (63.6 – 64.8 wt.% SiO<sub>2</sub>), which are the most differentiated eruptive  
493 products found at the CCVC (Fig. 10a, b, c). The mineral assemblage of Piribuela is  
494 composed of plagioclase (9 Avg. of Vol. %), amphibole (8 Avg. of Vol. %), biotite  
495 (altered crystals substituted by Fe-Ti oxides), and scarce pyroxene phenocrysts (1  
496 Avg. of Vol. %). At least two mono-lithological, matrix-supported breccias, with a high  
497 percentage of dacitic lithics (~40 vol.%), were identified east-ward of the domes,  
498 overlying the NE-DAD at the Imantag to Piribuela road (red hatched area in Fig. 2,  
499 Appendix figure C.2), and interpreted as related to a young-looking scar present at  
500 the south-eastern flank of the dome (Fig. 4c). These deposits have an estimated  
501 thickness of 20-30 m, reaching 6-7 km from their inferred source, and covering a  
502 surface of 7-8 km<sup>2</sup>. A sample of a dacitic juvenile block from this deposit yielded an  
503 age of  $65 \pm 2$  ka (COTA26, Table 1a).

504

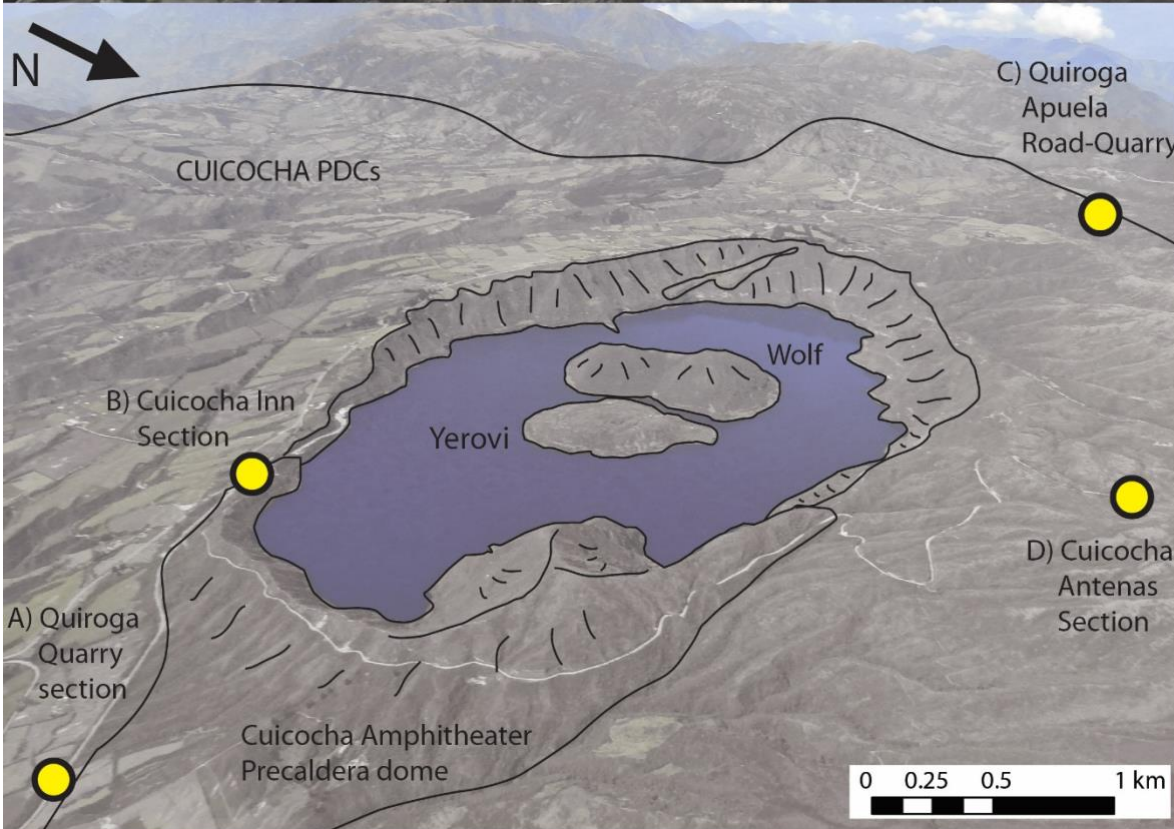


505 ***Cuicocha member***

506 *Pre-caldera unit (Ho-CuiD)*

507 The pre-caldera unit is composed of two sub-units, which correspond to the relicts  
508 of the Cuicocha pre-caldera dome (red unit in Fig. 2, Fig. 4d), and some mono-  
509 lithological volcanic breccias. Both are covered by a horizontal and compacted  
510 deposit of orange-coloured fine-grained ash. This ash deposit shows a proximal  
511 thickness of about 1 m decreasing to less than 5 cm at 16 km of distance.

512



515 *Figure 7. Aerial photograph of the Cuicocha caldera. The remnants of the pre-caldera dome are*  
516 *observed, as well as the lake, the caldera rim, and the Wolf and Yerovi post-caldera domes. The*  
517 *yellow circles represent the location of stratigraphic sections presented in figure 8 and sampling points*  
518 *for radiocarbon ages (results are given in Table 1b).*

519

520 *Pre-caldera dome:* The most representative outcrops of the pre-caldera dome relicts  
521 were identified in the caldera lake inner north-eastern walls and outside the caldera  
522 (south-eastern flank) of Cuicocha, covering an estimated area of 1.7 km<sup>2</sup>. Cuicocha  
523 dome also constitutes the highest point in the caldera border (3377 m). Cuicocha  
524 pre-caldera dome relicts display sub-vertical lava joints, which are light-grey  
525 siliceous andesites (58.1 - 62.8 wt.% SiO<sub>2</sub>), with a mineral assemblage of  
526 plagioclase (14 vol. %) and amphibole (6 vol. %). Fe-Ti oxides are found replacing  
527 almost entirely some amphibole phenocryst. Occasionally, a small percentage of  
528 clinopyroxene (1 vol. %) is present in these rocks (Fig. 9). A sample of unaltered  
529 lava from the dome yielded a poorly defined K-Ar age due to its very small radiogenic  
530 argon (<sup>40</sup>Ar\*) content (< 0.1%, Table 1a), but indicates that the dome was emplaced  
531 during Late Holocene times.

532 *Proximal monolithic breccia:* A relatively thin (1-2 m thick) layer of poorly sorted,  
533 matrix-supported breccia with a high percentage of dacite lithics (40-50 vol.%) and  
534 a dark-grey coloured, coarse-grained ash matrix covers the remnants of Cuicocha  
535 pre-caldera dome. This deposit is visible on the dome's southern flank, along the  
536 road that leads to the community of Apuela (1 km from the turn-off that leads to the  
537 entrance to the Cuicocha caldera lake, Fig. 8b), and at the inner walls of the southern  
538 caldera border.

539 At more distal outcrops (i.e., ~ 6 km westward along the same road), this matrix-  
540 supported breccia is observed to have a reduced percentage of porphyritic dacitic  
541 lithics (20-25 vol.%), as well as a dark grey to dark brown-coloured, medium-to-  
542 coarse-grained reworked ash matrix (< 2 mm size).

543

544 *Syn-caldera deposits (Ho-Cui)*

545 The syn-caldera deposit succession is composed of two volcanoclastic subunits that  
546 cover and smoothen the topography around Cuicocha lake (light green unit in Fig 2,

547 Fig. 8a). The syn-caldera deposit covers an area of  $66.6 \pm 0.1 \text{ km}^2$  and reaches as  
548 far as 13 - 15 km from the caldera lake towards the southeast (i.e., Hostería  
549 Cuicocha entrance, Quiroga quarries, between 3000 to 2500 m asl, Fig. 8c), and 3 -  
550 4 km to the northwest (i.e., road from Cuicocha lodge to Muyurcu dome, between  
551 3000 to 3300 m asl). Other thinner deposits were found to the north over the  
552 moorland (i.e., Las Antenas Road, between 3000 and 3900 m asl, Fig. 8d), reaching  
553 3-4 km up the slope of the southern flank of Cotacachi.

554 The subunits are a basal and voluminous sequence of pumice-and-ash pyroclastic  
555 density current deposits overlain by a less-voluminous layer of surge deposits.

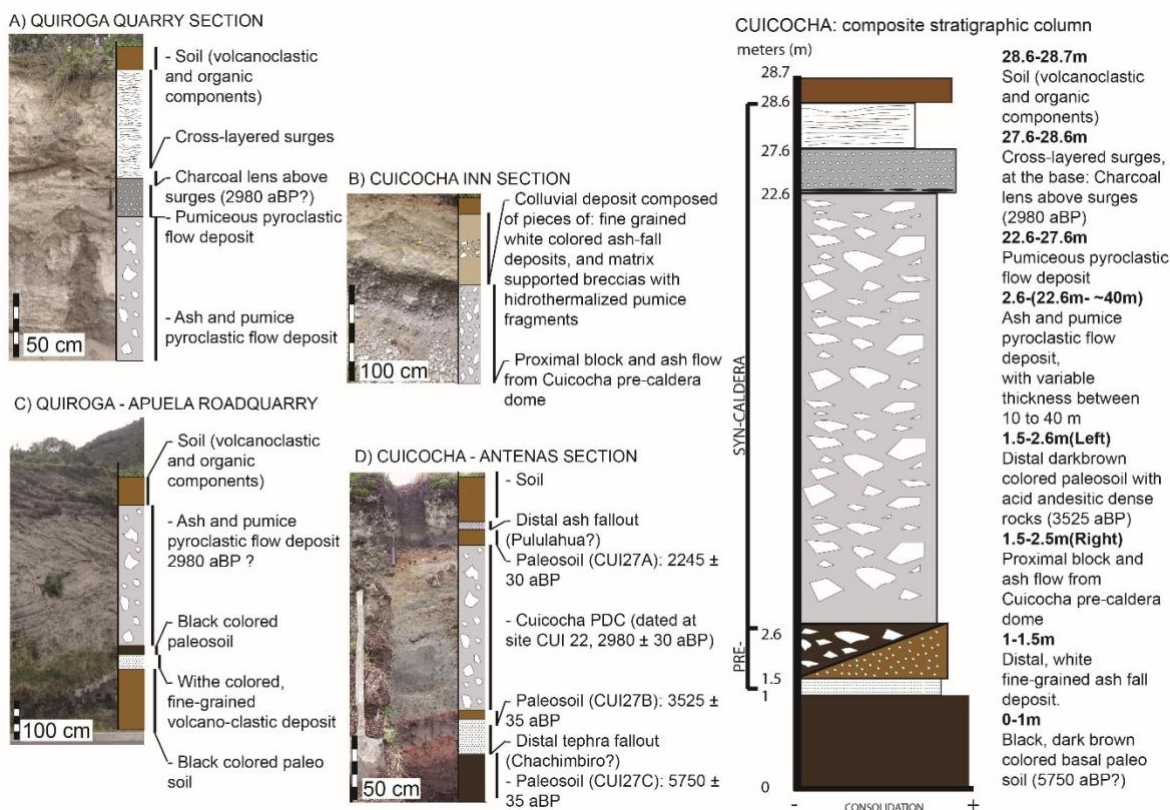
556 This syn-caldera pyroclastic succession overlays the pre-caldera units, and partially  
557 covers the southern flanks of the Cotacachi basal member (Fig. 8).

558 *Pyroclastic density current (PDC) deposits:* This subunit is a 5 to 40 m-thick (average  
559 of 20 m) succession of PDC deposits, formed by several pulses of caldera-forming  
560 explosive activity. In the field, each pulse can be identified by its pink-coloured top,  
561 which delimits PDCs horizons. At least 3 PDC layers are visible in the thickest  
562 outcrops such as Quiroga quarry, located 7 km to the south-east from the caldera  
563 lake. These deposits contain 30 vol. % of siliceous andesitic sub-angular pumice  
564 lapilli and blocks (61.8 – 62.7 wt. %  $\text{SiO}_2$ ), supported in a matrix of light grey-  
565 coloured, medium-grained ash, which includes free plagioclase and hornblende  
566 crystals. Similarly, the pumice mineral assemblage is plagioclase (9 Avg. of Vol. %),  
567 amphibole (8 Avg. of Vol. %). In addition, dense lithics of Cuicocha pre-caldera dome  
568 were found to make up at least 5 vol. % of these PCD deposits.

569 *Surge deposits:* Several pyroclastic surge deposits (i.e., dilute pyroclastic current  
570 deposits) less than 1 m thick overlay the PDCs layers. They display a cross-bedded  
571 stratification, are poorly sorted and fine-grained containing < 3 cm-size pumice lapilli  
572 (and accretionary lapilli; Pidgen, 2014) and light-grey fine-grained ash. The juvenile  
573 lapilli-pumice clasts have a siliceous andesitic composition (62.1 – 62.4 wt. %  $\text{SiO}_2$ ).  
574 Less than 3 vol. % of dense siliceous andesites from the pre-caldera dome  
575 composed of plagioclase, amphibole, and scarce biotite were also incorporated.

576 Different centimetre thick reworked volcanoclastic layers are interspersed within this  
577 succession between the pyroclastic flows and the pyroclastic surges, especially in

578 the moor area. Radiocarbon dating (Table 1b) of charcoal and soil samples found  
 579 within Cuicocha syn-caldera deposits yields ages of  $3525 \pm 35$  aBP (CUI-27B) at the  
 580 base and  $2980 \pm 30$  aBP (CUI-22B) at the top of the pyroclastic flows, which is  
 581 concordant with the ages obtained by von Hillebrandt. (1989), of  $2990 \pm 300$  a BP  
 582 (Table. 1b).  
 583



584  
 585 *Figure 8. A B, C, and D are different stratigraphic sections of Cuicocha Caldera. To the right:*  
 586 *Composite stratigraphic column of the section of the Cuicocha member. Note the stratigraphy*  
 587 *section's location at figure 7. All the dates here presented belongs to this study, see table 1b.*

588  
 589 *Post-caldera unit, Wolf and Yerovi domes (PC)*

590 This unit comprises four coalescent domes emplaced inside the Cuicocha caldera  
 591 lake (Fig. 2, Appendix figure C.3), which form two volcanic islets called Wolf  
 592 (maximum slopes of  $48^\circ$ ) and Yerovi (maximum slopes of  $35^\circ$ , see section 4.1 for  
 593 morphology and structure). The rocks that compose these domes are porphyritic  
 594 siliceous andesites ( $61.5 - 62.2$  wt.%  $\text{SiO}_2$ ) bearing phenocryst of plagioclase (14  
 595 Avg. of Vol. %), amphibole (12 Avg. of Vol. %), inside a glassy matrix. These domes

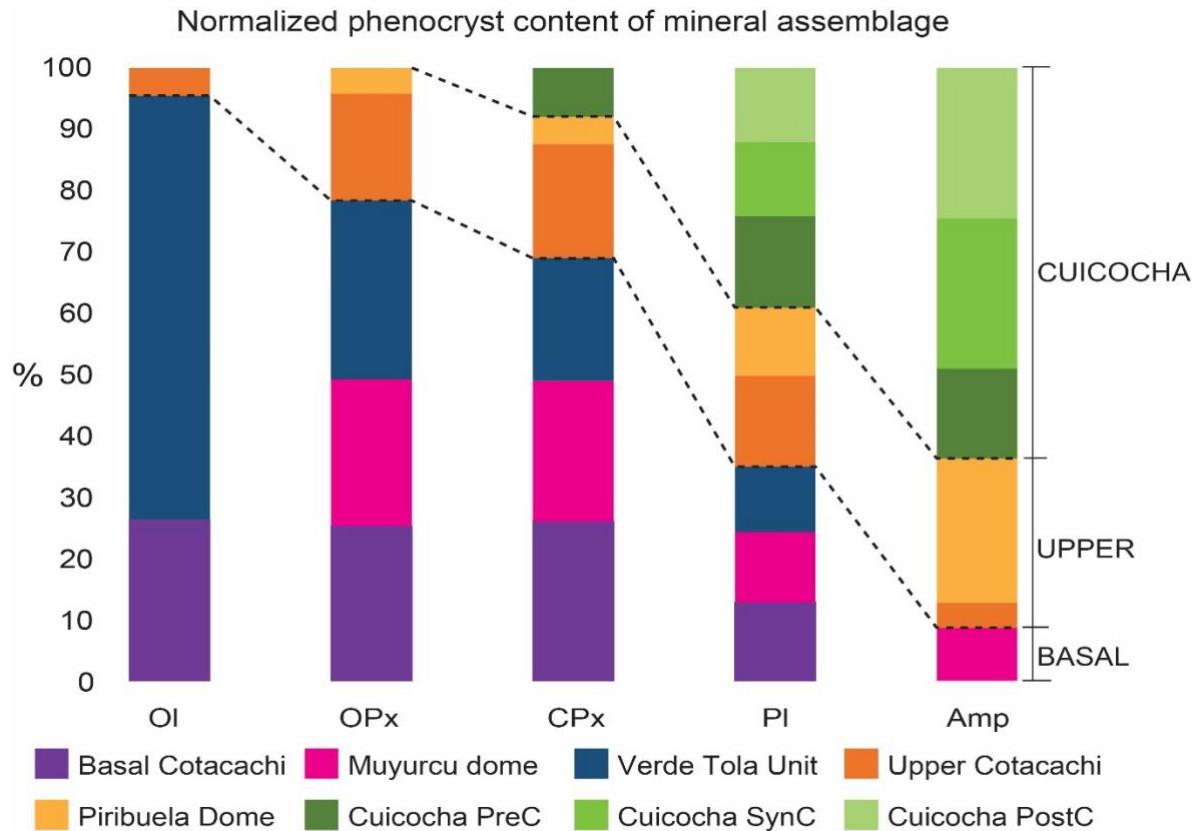
596 were emplaced after caldera formation, which means that they are younger or  
597 coetaneous than  $2980 \pm 30$  aBP (CUI-22B) (Table 1b).

598

#### 599 **4.4. Main petrographic and geochemical characteristics**

600 The textures of the rocks that form the central edifice of Cotacachi are glomero-  
601 porphyritic to ophitic, with mostly euhedral shaped phenocrysts, while the rocks that  
602 form the domes and the products of Cuicocha Caldera are porphyritic with trachytic  
603 texture. In both cases, the matrix is constituted by glass and microlites of plagioclase  
604 ( $< 100 \mu\text{m}$ ) and amphibole (for Cuicocha, Piribuela, and few in Muyurcu). Plagioclase  
605 constitutes the dominant crystals, present in a similar percentage (11 – 12 vol. %) in  
606 all stratigraphic members of the CCVC. On the contrary, the presence of olivine and  
607 amphibole crystals is not homogeneous. The amount of olivine in the rocks of the  
608 basal lava flows (2 vol. %) progressively decreases as the rocks become more silica-  
609 rich (Upper member), to fully disappear at Piribuela dome and Cuicocha member  
610 (Fig. 9, Appendix table B.1). The opposite is true for the amphibole phenocrysts,  
611 which progressively appear in the upper Cotacachi lava successions (4 vol.%),  
612 reaching a considerable content in the peripheral domes (Fig. 9), especially at  
613 Cuicocha (8 vol.%).

614



615

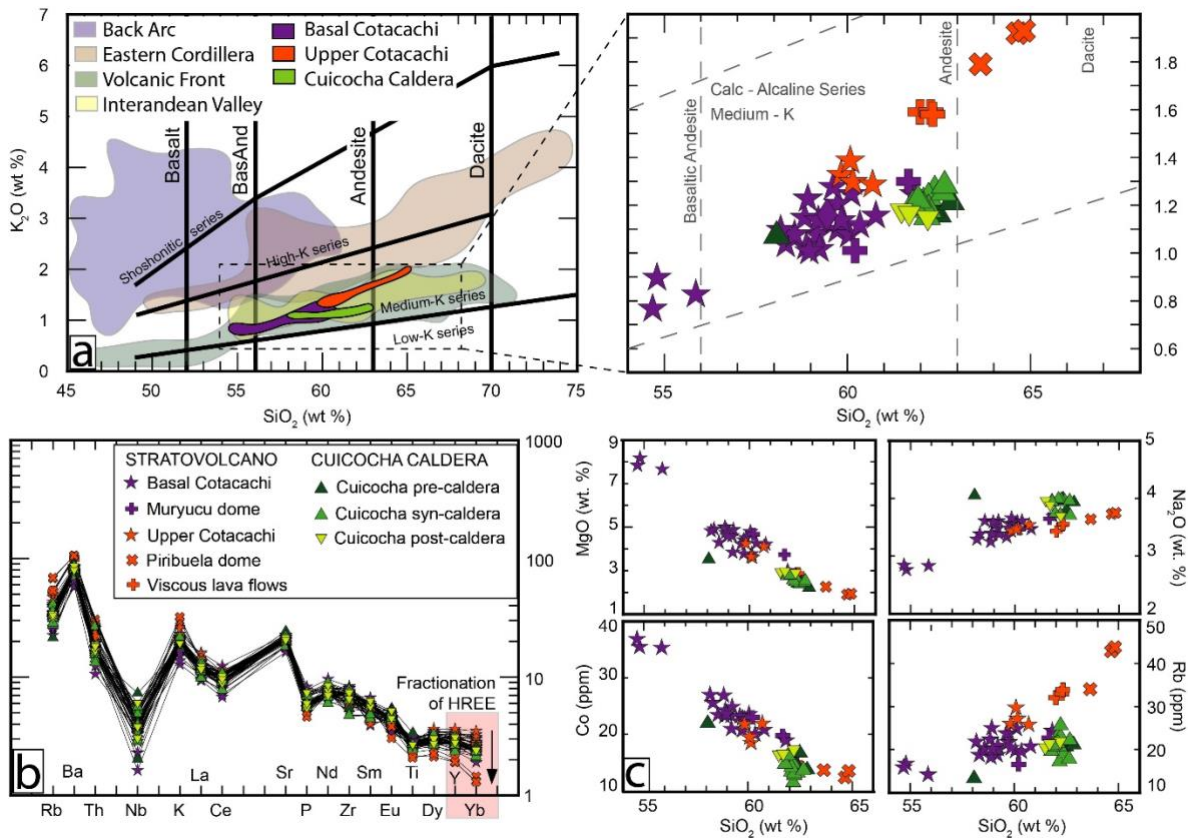
616 *Figure 9. Variability of Cotacachi - Cuicocha mineral assemblages in a base of a phenocryst*  
 617 *normalization, see Appendix table B.1, note the transitional mineralogical change from Basal*  
 618 *Cotacachi to Upper Cotacachi and Cuicocha member. Amp: amphibole, Pl: plagioclase, Cpx:*  
 619 *clinopyroxene, Opx: orthopyroxene, Ol: olivine.*

620

621 CCVC rocks are calc-alkaline medium potassium basic to acidic andesites and  
 622 dacites (54.68 – 64.83 wt.% SiO<sub>2</sub>, 0.8 – 1.9 wt. % K<sub>2</sub>O, Appendix table B.2)  
 623 (Peccerillo and Taylor, 1976; Fig. 10a). They fall into the field of other erupted rocks  
 624 produced in the Ecuadorian Western Cordillera (Hidalgo et al., 2012; Ancellin et al.,  
 625 2017). In the primitive mantle normalized multi-elements diagram (Fig. 10b), all  
 626 CCVC rocks display the Nb-negative anomaly and enrichments in Large Ion  
 627 Lithophile Elements (LILE) as Rb, Ba, Th and K, typical of calc-alkaline rocks. A  
 628 slight negative anomaly is also observed for P, while Heavy Rare Earth Elements  
 629 (HREE) show mostly a flat pattern. Few samples from Cotacachi show a highly  
 630 fractionated spectrum specially for Yb (Fig. 10b).

631 Major elements such as MgO, FeO, and CaO show negative correlations with silica,  
 632 while Na<sub>2</sub>O and K<sub>2</sub>O show positive ones (Fig. 10c) as well as transition metals such

633 as Co, Ni, Cr, and Sc, show a compatible behaviour, illustrated by the Co vs. SiO<sub>2</sub>  
 634 diagram in figure 10c. In contrast, the Light Rare Earth Elements (LREE, e.g., Ce,  
 635 La), and some Large Ion Lithophile Elements (LILE, e.g., Rb, Ba), show incompatible  
 636 behaviour, illustrated by the Rb vs. SiO<sub>2</sub> diagram (Fig. 10c). Th, Rb, La, and Ba in  
 637 Cuicocha rocks follow the same pattern as K<sub>2</sub>O.  
 638



639  
 640 *Figure 10. a) Left: K<sub>2</sub>O vs. SiO<sub>2</sub> diagram from Peccerillo and Taylor (1976) for representative samples*  
 641 *of the Ecuadorian Volcanic Arc (modified from Hidalgo et al., 2012). The CCVC samples are*  
 642 *highlighted. Right: Zoom to CCVC K<sub>2</sub>O vs. SiO<sub>2</sub> members and units. b) Diagram of trace element*  
 643 *content of CCVC rocks normalized to the primitive mantle (Sun and McDonough, 1989), note the high*  
 644 *fractionation of the HREE (e.g., Yb) highlighted in the red-colored square. c) Representative Harker*  
 645 *diagrams (MgO, Na<sub>2</sub>O, Co and Rb) of CCVC members and units.*

646

647 **4.5. Bulk volumes and eruptive rates**



648 *Bulk volumes*

649 Results obtained using the interpolation MatLab script (see Andrade et al., 2021)  
 650 with input surface values of  $107 \pm 3 \text{ km}^2$  and heights ranging between 2519 and  
 651 4939 m asl, yield an estimated minimum bulk volume of  $56 \pm 4 \text{ km}^3$  for all CCVC  
 652 proximal eruptive products currently remaining (i.e., the non-eroded volume; Fig. 11),  
 653 where the  $\pm 4 \text{ km}^3$  represent the standard deviation of the analytical results. However,  
 654 to reduce the uncertainty of this method we must consider an error of  $\pm 2\%$  in the  
 655 cartographic boundary used by the script, which can modify the resulting volume by  
 656 up to  $\pm 10 - 20 \%$ . Applying the ShapeVolc reconstruction method (Lahitte et al.  
 657 2012), we calculated a minimum bulk volume of emitted material of  $91 \pm 25 \text{ km}^3$  for  
 658 the end of the CVCCs main construction stage (approx. 100 ka). The difference  
 659 between the current ( $56 \pm 4 \text{ km}^3$ ) and the reconstructed volume ( $91 \pm 25 \text{ km}^3$ ) is  $36$   
 660  $\pm 9 \text{ km}^3$ , which represents the eroded volume since the end of the construction of  
 661 the Upper Cotacachi, i.e., during the last 100 ka, which defines an erosion rate of  
 662  $0.3 \pm 0.1 \text{ km}^3/\text{kyr}$  (Table 2b). We can assume a similar average erosion rate for both  
 663 periods, since the syn-construction and post-construction periods (i.e.,  $173 \pm 4$  to  
 664  $108 \pm 6 \text{ ka}$ , and after  $108 \pm 6 \text{ ka}$ , respectively) both experienced a full glacial-  
 665 interglacial cycle, and the average volume of the volcanic complex during these two  
 666 stages is comparable. Therefore, applying the post-construction erosion rate of  $0.3$   
 667  $\pm 0.1 \text{ km}^3/\text{kyr}$  to the syn-construction period of the basal and Upper Cotacachi  
 668 members, the volume eroded between  $173 \pm 4$  and  $108 \pm 6 \text{ ka}$  is estimated at  $21 \pm$   
 669  $6 \text{ km}^3$ . Finally, by adding this syn-construction eroded volume to that reached by the  
 670 volcano at the end of its construction stage ( $91 \pm 25 \text{ km}^3$ ), we obtain a total erupted  
 671 volume of  $112 \pm 31 \text{ km}^3$  for the uneroded Cotacachi basal and upper edifices (100ka  
 672 stage, Fig. 11b).

673

a	Unit	Surface ( $\text{km}^2$ )	Extrapolated max. Volume ( $\text{km}^2$ )	Estimated minimum bulk Volume ( $\text{km}^3$ )	Estimated Volume ( $\text{km}^3$ )	Estimated Volume thick (m)	Estimated Volume thick (m)	Estimated average thick (m)	Maximum length (m)
	Basal Cotacachi	107.3			$49 \pm 4$				
NW DAD	12	63		$0.5 \pm 0.2$	$1.1 \pm 0.1$	66	24	45	40
Muyurcu dome	2.4			0.3					
Loma Negra dome	1.9			0.1					

Upper Cotacachi	16.2			1.7					
NE DAD	12	41	$0.2 \pm 0.1$	$1.8 \pm 0.5$	20	16	18	30	
Piribuela dome	3.6			0.3					
Cuicocha pre-caldera	1.6			0.1					
Cuicocha syn-caldera	66.6			4.1					
Cuicocha post-caldera	0.8			0.04					
					Cuicocha total Volume (km <sup>3</sup> )	56 ± 4	Cuicocha total volume (km <sup>3</sup> )	4.2 ± 0.1	

674

b	Stage	Age max.	Age min.	Period	Raw volume	Eroded volume	Total, volume	Eruptive rate		Erosion rate	
		ka	ka	ka	km <sup>3</sup>	km <sup>3</sup>	km <sup>3</sup>	km <sup>3</sup> /kyr	mm/yr	km <sup>3</sup> /kyr	mm/yr
	Construction Basal + Upper Cotacachi	173 ± 4	108 ± 6	65 ± 7	91 ± 25	21 ± 6	112 ± 31	1.7 ± 0.5	7.4 ± 2.2		
	Erosion since the end of Upper cotacachi construction	108 ± 6	0	108 ± 6			36 ± 9			0.3 ± 0.1	1.4 ± 0.4

675

676 *Table 2. a) Volume estimations in base of a MatLab interpolation using the 4m resolution digital*  
677 *elevation model (Instituto Geográfico Militar - IGM). b) Result of volumes, eruptive and erosion rates*  
678 *calculations obtained from ShapeVolc software (Lahitte et al., 2012) and given at 1-sigma accuracy.*

679

680 Due to the high erosion rate, the NW and NE debris-avalanche deposits are found  
681 scattered in form of isolated terraces in the Intag and Ambi river valleys (Appendix  
682 figure B), respectively. In addition, the traces of the supposed corresponding scars  
683 in the higher flanks have been strongly eroded, impeding any avalanche volume  
684 calculations based on the scar sizes (Appendix figure B). Therefore, minimum  
685 volumes were calculated for the currently observed remaining debris-avalanche  
686 deposit terraces, while maximum volumes were estimated by extrapolating the  
687 potentially eroded deposit surface and using average thickness values of 45 and 18  
688 m for the NW- and NE-DAD, respectively. In this manner, for the NW-DAD, which is  
689 found between 3282 and 1960 m asl, we obtained volumes between  $0.5 \pm 0.2$  km<sup>3</sup>  
690 and  $1.8 \pm 0.5$  km<sup>3</sup>, covering a surface of 12 to 41 km<sup>2</sup>, respectively. For the NE-DAD,  
691 found between 2315 to 1637 m asl, the estimated volumes range from  $0.2 \pm 0.1$  km<sup>3</sup>  
692 to  $1.1 \pm 0.1$  km<sup>3</sup>, covering surfaces of 12 to 63 km<sup>2</sup>, respectively.

693

694 For Cuicocha deposits, a current bulk volume of  $4.2 \pm 0.1$  km<sup>3</sup> was obtained using  
695 the MatLab interpolation script including the pre-, syn- and post-caldera deposits,  
696 which cover a surface of 68 km<sup>2</sup>, with a variable altitude from 2535 to 3910 m asl.

697 This volume value agrees with the minimum volume of  $4.1 \text{ km}^3$  estimated by von  
698 Hillebrandt (1989). In addition, tephra fallout deposits of Cuicocha cover a surface  
699 of approximately  $6.8 \times 10^2 \text{ km}^2$ , reaching the northern Ecuadorian coastline 176 km  
700 away from the volcano. A volume estimation based on the Legros (2000) method for  
701 a single isopach, results in  $2 \text{ km}^3$  of tephra fallout, using a representative thickness  
702 of 0.08 m (calculation detailed in Vallejo Vargas, 2011).

703

#### 704 *Eruptive rates*

705 A minimum bulk emission rate of  $1.7 \pm 0.5 \text{ km}^3/\text{ka}$  for the main basal Cotacachi lava  
706 flows, was obtained using the step times of 65 ka (Cotacachi stratovolcano).

707 If we include the last age (2.98 ka) corresponding to the Cuicocha eruption ( $4.2 \text{ km}^3$ ),  
708 we obtain an emission rate of  $0.068 \pm 0.016 \text{ km}^3/\text{ka}$  (pause time of 62 ka, since the  
709 formation of the Piribuela dome until the Cuicocha pre-caldera dome development),  
710 corresponding to this last period of CCVC construction. Such drop in Cotacachi  
711 volcano bulk emission rate from  $1.7 \pm 0.5$  to  $0.068 \pm 0.016 \text{ km}^3/\text{ka}$  indicates a  
712 progressive decrease in its eruptive activity.

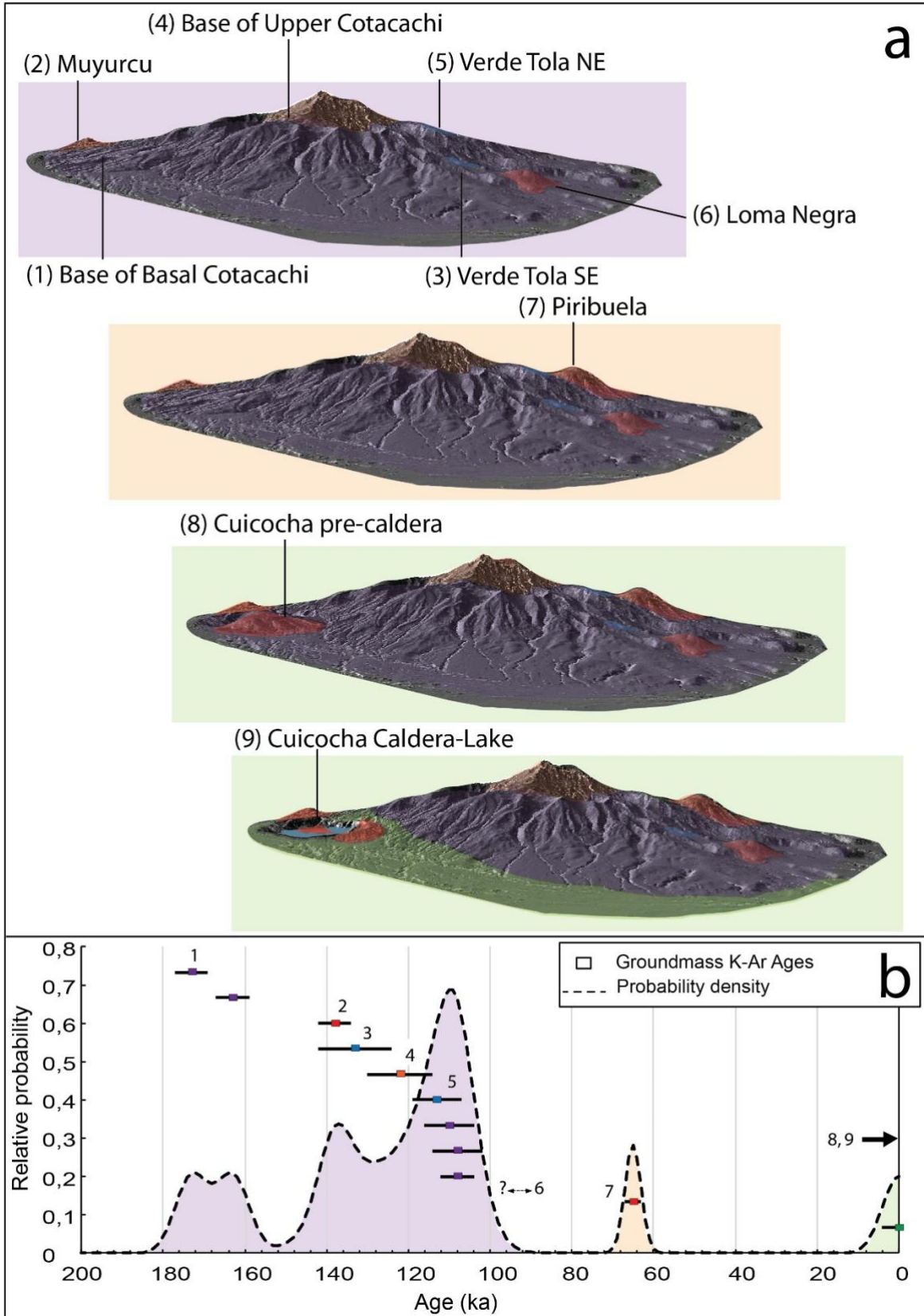
713

## 714 **5. DISCUSSION**

### 715 **5.1. Chronological evolution of CCVC**

716 According to the chronology obtained during this study, the eruptive activity of the  
717 CCVC suggest this volcanic centre is among the youngest of the Western Cordillera  
718 of the Ecuadorian Andes. Indeed, the Cotacachi stratovolcano ( $173 \pm 4$  to approx.  
719 15 ka; this study, Fig. 11a) is younger than Cushnirumi ( $411 \pm 8$  to  $383 \pm 6$  ka; Bablon  
720 et al., 2020), Mojanda ( $1038 \pm 87$  to  $194 \pm 6$  ka; Bablon et al., 2020) and Cusin ( $517$   
721  $\pm 8$  to  $495 \pm 12$  ka; Bablon et al., 2020). It is contemporary to the development of  
722 Fuya Fuya ( $476 \pm 38$  to  $28 \pm 5$  ka; Bablon et al., 2020), Chachimbiro (approx. 405 to  
723 5 ka; Bernard et al., 2014, Bellver-Baca et al., 2019, Bablon et al., 2020), Cubilche  
724 ( $45 \pm 5$  to  $40 \pm 5$  ka; Navarrete et al., 2020, Bablon et al., 2020), and Imbabura ( $47$   
725  $\pm 6$  to approx. 8 ka; Le Pennec et al., 2011, Andrade et al., 2019, Bablon et al.,  
726 2020). Finally, the Cuicocha ( $3525 \pm 35$  aBP to  $2980 \pm 30$  aBP) explosive volcanism  
727 is one of the youngest in the northern part of the Ecuadorian Andes together with

728 Pululahua Dome Complex dated at approx. 2600-2300 aBP (Andrade et al, 2021;  
729 Vásquez Müller et al., 2022).



731 *Figure 11. a) Morphological and chronological reconstruction of Cotacachi-Cuicocha Volcanic*  
732 *Complex. b) Gaussian Age-probability spectrum (calculation detailed in Deino and Potts, 1992),*  
733 *outlining potential gaps of activity between 100 and 65 ka, and between 65 and ~4 ka. Groundmass*  
734 *K-Ar ages are shown with the same color used for units from figure 2.*  
735

### 736 *Cotacachi strato-volcano*

737 The age probability curve (Fig. 11b) calculated from the K-Ar ages obtained here for  
738 the volcanic complex shows six peaks of activity, with three growth gaps. It highlights  
739 the formation of the basal stratovolcano (Cotacachi) between 180 and 100 ka. Within  
740 this interval, the first short hiatus of activity is followed by the extrusion of the  
741 southwest Muyurcu dome and the subsequent emission of lavas from the Verde Tola  
742 unit (SE: 133 ka and NE: 113 ka). The younger construction phase of the Cotacachi  
743 strato-volcano occurred between 122 and 108 ka. The following two stages of activity  
744 (70 to 60 ka, and less than 10 ka, respectively) are associated with the extrusion of  
745 the Piribuela (the most silica-rich dome of CCVC; dated at 65 ka) and Cuicocha  
746 domes. Nevertheless, we must keep in mind that such age-probability curve is  
747 biased by the low number of available ages, mostly due to the lack of sample from  
748 difficult-to-access units (e.g., summit lava flows). Note that the plagioclase (CUI-30A)  
749 age of  $207 \pm 25$  ka is much older than the age obtained from the groundmass of the  
750 same sample (Table 1a). This suggests that, as observed elsewhere (e.g., Singer et  
751 al., 1998), plagioclase crystals could have been incorporated in the magma reservoir  
752 and did not have time to be reset before the eruption. This led to an apparent K-Ar  
753 age older than the age of the eruption. This example supports the importance of  
754 carrying K-Ar ages on groundmass for young volcanic material.

755 The main cone-building stage (Middle to Upper Pleistocene, starting at  $173 \pm 4$  ka)  
756 of the Cotacachi cone is represented by the emission of a thick succession of  
757 andesitic lava flows, which form the lower and middle flanks of the edifice,  
758 constructed directly over the Cretaceous to Paleocene basement of the Western  
759 Cordillera. Some peripheral domes were formed subsequently, starting with the  
760 oldest south-western Muyurcu, at about 140 ka. Stratigraphic relationships show that  
761 the south-eastern Loma Negra dome is younger than  $108 \pm 6$  ka. During the period  
762 between 140 and 108 ka, the lava flows of Verde Tola were emitted, the composition  
763 (54.7 - 55.9 wt.% SiO<sub>2</sub>) of which suggests an apparent effusive type of activity,

764 forming two isolated (SE:  $133 \pm 9$  ka, NE:  $113 \pm 6$  ka) olivine-bearing and  
765 magnesium-rich basaltic-andesitic lava flow successions. A 5 km large amphitheatre  
766 that opens to the NW cuts the basal lava flows of Cotacachi. The corresponding  
767 debris avalanche deposits reach approx. 40 km along the Intag valley and are  
768 characterized by the absence of amphibole-bearing andesites, which is typical for  
769 the Upper Cotacachi member. Based on the description we suggest this first north-  
770 western debris avalanche occurred before  $108 \pm 6$  ka.

771 The upper and steep flanks of the Cotacachi stratocone represent the last phase of  
772 development of the main cone-building stage (Cotacachi upper member). The  
773 youngest ages of the Basal member ( $110 \pm 6$  and  $108 \pm 6$  ka), overlap the oldest  
774 age ( $122 \pm 8$  ka) of the Upper lava flow succession (Appendix figure C.1), which can  
775 be interpreted as the loss of the youngest section of this building stage, due to the  
776 intense erosion rate we have obtained here ( $0.3 \pm 0.1$  km<sup>3</sup>/kyr). The second partial  
777 flank collapse event occurred on the north-eastern flank, leaving a debris avalanche  
778 (NE-DAD) deposit that crops out towards the Ambi river valley and is covered by the  
779 Piribuela deposits at the proximal facies and by the Imbabura DAD at its distal facies  
780 (Appendix figure C.2). Interaction between the avalanche and the glacier has had an  
781 important implication in the fluidization of the moving mass (Deline, 2009) of the NE-  
782 DAD, giving the deposit an appearance of a big lahar. Since Piribuela dome was not  
783 affected by the debris avalanche event and its associated deposits overlay the NE  
784 avalanche, the NE-DAD must have taken place between  $108 \pm 6$  and  $65 \pm 2$  ka.  
785 Following the discrimination between volcanic debris and rock avalanches (Dufresne  
786 et al., 2021), we have tried to establish the origin of those observed at CCVC. Due  
787 to the low juvenile clast content as well as the apparent structural control provided  
788 by the Billecocha fault system, we propose that the debris avalanche events at  
789 CCVC originated from tectonic disturbances rather than from violent eruptions. The  
790 last evidence of eruptive activity of Cotacachi edifice corresponds to the summit lava  
791 flows (Fig. 4e, Fig. 5a), which lack glacial erosion, suggesting an age younger than  
792 the LGM (i.e., from 33 to 14 ka; Clapperton, 1990; Samaniego et al., 2012; Bablon  
793 et al., 2019). In addition, Ego et al. (1996) suggests a specific period of activity for  
794 the Billecocha fault system between 5.7 and 10 ka BP. Considering that the summit

795 lava flows have not been affected by the regional tectonics, Cotacachi activity could  
796 have lasted until 15 - 10 ka BP. Cuicocha pre-caldera dome ( $^{14}\text{C}$ :  $5750 \pm 35$  aBP to  
797  $3525 \pm 35$  aBP; Table. 2b), is the youngest volcanic dome in the evolution of the  
798 CCVC, whose destruction resulted in the formation of the Cuicocha caldera lake.

799

#### 800 *Cuicocha explosive event*

801 The caldera-forming eruption of Cuicocha is characterized by a large succession of  
802 pyroclastic density currents (i.e., pumice and ash pyroclastic flows, and surges) that  
803 covers a large surface ( $67 \text{ km}^3$ , Table 2a) around the caldera (von Hillebrandt, 1989;  
804 Pidgen, 2014; Fig. 2, Fig. 7).

805 This explosive phase (Syn-caldera unit) is related to the destruction of the pre-  
806 caldera Cuicocha dome and the formation of the first crater/depression. Successions  
807 of poorly stratified pyroclastic-flow deposits are related to the paroxysmal phase of  
808 the eruption (Pidgen, 2014). Additionally, the physical characteristics of Cuicocha  
809 surge deposits (i.e., highly fragmented, fine-grained deposits, presence of  
810 accretionary lapilli, and cross/layered stratification) reveal that an intense  
811 phreatomagmatic activity took place during a new dome construction phase in a  
812 subaqueous environment (i.e., inside the first caldera lake) ( $^{14}\text{C}$ :  $2980 \pm 30$  aBP).

813 The Cuicocha eruption ended with the formation of the Wolf and Yerovi post-caldera  
814 domes (von Hillebrandt, 1989; Pidgen, 2014). The volumes of  $4.2 \pm 0.1 \text{ km}^3$  and  $\sim 2$   
815  $\text{km}^3$  obtained for the proximal PDC deposits and tephra fallout deposits, respectively,  
816 classify this event with a Volcanic Explosivity Index of 5 (VEI= 5; Newhall and Self,  
817 1982). Our data suggest that the pre-caldera lava dome formation, the syn-caldera  
818 explosive phase, and the post-caldera dome growth of Cuicocha, occurred during a  
819 period spanning roughly 1.5 ka, probably involving more than one eruptive event.

820 The resulting morphology produced by the above-described phenomena is a funnel-  
821 shaped caldera, which main characteristic is their shape, resulting from the outward  
822 widening of the vent, through erosive and gravitational mechanisms, such as  
823 progressive subsidence of a highly fractured crater (Lipman, 2000; Cole et al., 2005).

824 Future work should address the formation of the observed Cuicocha depression in  
825 more detail since the present interpretations are based on its morphology.



826

827 **5.2. Contextualizing volumes, erosion, and eruptive rates**

828 The erupted volume corresponds to the difference between the basement elevation  
829 interpolation and the elevation model at the end of CCVC construction, while the  
830 post-construction eroded volume corresponds to the difference between the  
831 elevation model at the end of edifice construction and the present-day morphology.  
832 As detailed in Bablon et al. (2018), eruptive rates were calculated using durations  
833 derived from age differences between the beginning and the end of the main  
834 construction stages, whereas post-activity erosion rate calculations involved the time  
835 elapsed since the end of Cotacachi construction. Then, although both methods have  
836 allowed estimating volumes, their limitation lies in the quantification of the cause-  
837 effect produced by loss of data (Andrade et al., 2021; Vásconez Müller et al., 2022).  
838 In this sense, estimated volume should be considered with caution and are  
839 presented with a high uncertainty due to biases that can be induced by erosion (loss  
840 of data from younger sequences), modelling of the basement elevation, as well as  
841 the possible flank collapses.

842

843 By comparing the bulk volume results obtained for the current and the reconstructed  
844 Cotacachi-Cuicocha Volcanic Complex (56 vs. 91 km<sup>3</sup>) with those of other andesitic  
845 - dacitic volcanic complexes in the Ecuadorian arc (Pichincha volcanic complex: 30  
846 to 250 km<sup>3</sup>, Robin et al., 2010; Chimborazo: 63 to 100 km<sup>3</sup>, Samaniego et al., 2012;  
847 Imbabura: ~ 65 km<sup>3</sup>, Cushnirumi: ~53 km<sup>3</sup>, Bablon et al., 2020) and others with  
848 similar characteristics in the Andes (Ampato Sabancaya – Peru: 44 - 54 km<sup>3</sup>,  
849 Samaniego et al., 2016; El Misti – Peru: 70 km<sup>3</sup>, Thouret et al., 2001), we observe  
850 that the CCVC is among the more voluminous volcanoes of the Northern and Central  
851 Volcanic Zones of the Andes.

852 In contrast, the range of volumes obtained for the NW (0.5 – 1.8 km<sup>3</sup>) and NE (0.2 –  
853 1.1 km<sup>3</sup>) avalanches are smaller than other Ecuadorian avalanche deposits (i.e.,  
854 Sangay: ~33 km<sup>3</sup>, Valverde et al., 2021; Chimborazo: 10 – 12 km<sup>3</sup>, Samaniego et  
855 al., 2012; Tungurahua: 8 km<sup>3</sup>, Hall et al., 1999; Cubilche: 3 km<sup>3</sup>, Roverato et al.,

2018), as well as others from continental volcanoes (i.e., Saint Helens-USA: 2.5 km<sup>3</sup>, Voight et al., 1981; Oshima – Japan: 2.5 km<sup>3</sup>, Satake and Kate, 2001).

Moreover, we estimated that 36 ± 9 km<sup>3</sup> of material have been eroded since the end of Cotacachi construction (~100 ka), corresponding to an average erosion rate of 0.3 ± 0.1 km<sup>3</sup>/kyr. This erosion rate is one of the highest obtained in the Ecuadorian Andes, only comparable to those of Carihuairazo volcano (Samaniego et al., 2022), South Iliniza volcano (Santamaria et al., 2022) and the oldest stage of Tungurahua volcano (~0.2 ± 0.1 km<sup>3</sup>/kyr; Bablon et al. 2020). The high erosion rates in CCVC can be related to the combination of tectonic events with common erosion processes (such as glacial, fluvial and wind erosion) during its evolution.

Finally, the decrease observed for the CCVC's bulk emission rate, from 1.7 ± 0.5 for Cotacachi to 0.068 ± 0.016 km<sup>3</sup>/ka for Cuicocha, is similar to the case of Chimborazo volcano, which declines from 1.6 to 0.3 km<sup>3</sup>/ka, from the basal to the youngest cone, respectively (Samaniego et al., 2012).

871

872

## 873 **6. CONCLUSIONS**

874

The Cotacachi-Cuicocha Volcanic Complex (0.361° N; 78.349° W) is composed of a stratovolcano (Cotacachi: 173 ± 4 until the end of the Pleistocene), four peripheral/satellite domes (Muyurcu: 138 ± 4 ka; Loma Negra: younger than 108 ka; Piribuela: 65 ± 2 ka and Cuicocha pre-caldera: about 3 ka), and a funnel-shaped caldera, currently occupied by a lake, formed during a large explosive event dated at 2980 ± 30 a BP (4.2 ± 0.1 km<sup>3</sup> of emitted material) that ended with the extrusion of two post-caldera domes. Cuicocha is considered a potentially active volcano that is currently monitored.

883

CCVC rocks ranges from basic to siliceous andesites and dacites (54.7 – 64.8 wt.% SiO<sub>2</sub>), whose chemistry corresponds to medium potassium, calc-alkaline magmatic series and exhibits the typical trend of the rocks erupted at the Western Cordillera

887 and Inter-Andean Valley of the Ecuadorian Andes (Hidalgo, et al., 2012; Fig. 10).  
888 Cuicocha siliceous-andesites are slightly depleted in K<sub>2</sub>O and some trace elements  
889 such as Th, Rb, La, and Ba, displaying a different trend to that of Cotacachi  
890 stratovolcano and its peripheral domes. The mineral assemblage of the stratigraphic  
891 members (Basal and Upper Cotacachi, and Cuicocha) of CCVC shows a  
892 characteristic transition defined by the progressive disappearance of olivine and the  
893 appearance of amphibole and biotite as silica content increases.

894

895 The CCVC, is one of the youngest (Middle Pleistocene to Holocene), and largest  
896 (4939 m asl; 56 to 91 km<sup>3</sup> bulk volume) volcanoes in the northern Western Cordillera  
897 of Ecuadorian Andes. Due to its height, its high elevation, and its proximity to active  
898 faults, it has suffered a strong erosion (~0.3 km<sup>3</sup>/kyr), that should be linked to fluvial,  
899 wind, glacial, and tectonic processes. This erosion rate is among the most important  
900 of the entire Ecuadorian arc.

901

902 In addition, two small avalanches affected different volcano flanks (NW, along Intag  
903 valley, and NE, along Ambi river valley flanks, respectively) at different stages of its  
904 formation. The north-western avalanche (0.5 ± 0.2 to 1.8 ± 0.5 km<sup>3</sup>; older than 108  
905 ka) affected the Basal edifice, and the north-eastern avalanche (0.2 ± 0.1 to 1.1 ±  
906 0.1 km<sup>3</sup>; 108 – 65 ka) affected the Upper lava flow succession.

907

## 908 **7. ACKNOWLEDGEMENT**

909 The results presented in this work are the result of a long-lasting Ecuadorian French  
910 cooperation program, carried out between the Instituto Geofísico de la Escuela  
911 Politécnica Nacional (IG-EPN) through SENPLADES project (Generación de  
912 Capacidades para la Emisión de Alertas Tempranas), and the Institut de Recherche  
913 pour le Développement (IRD, France) through a “Laboratoire Mixte International”  
914 program entitled “Séismes et Volcans dans les Andes du Nord”. We deeply thank  
915 the anonymous reviewers and the Invited Editor, C. Vallejo, for their insightful  
916 comments that improve the manuscript.

917

918 **8. REFERENCES**

919

920 Alvarado, A., Audin, L., Nocquet, J. M., Jaillard, E., Mothes, P., Jarrín, P., Cisneros, D., 2016.

921 Partitioning of oblique convergence in the Northern Andes subduction zone: Migration history and  
922 the present-day boundary of the North Andean Sliver in Ecuador. *Tectonics*, 35(5), 1048-1065.

923 Ancellin, M. A., Samaniego, P., Vlastélic, I., Nauret, F., Gannoun, A., Hidalgo, S., 2017. Across-arc  
924 versus along-arc Sr-Nd-Pb isotope variations in the E Ecuadorian volcanic arc. *Geochemistry,*  
925 *Geophysics, Geosystems*, 18(3), 1163-1188.

926 Andrade, S. D., van Wyk de Vries, B., & Robin, C., 2019. Imbabura volcano (Ecuador): The influence  
927 of dipping-substrata on the structural development of composite volcanoes during strike-slip  
928 faulting. *Journal of Volcanology and Geothermal Research*, 385, 68-80.

929 Andrade, S. D., Müller, A. V., Vasconez, F. J., Beate, B., Aguilar, J., Santamaría, S., 2021. Pululahua  
930 dome complex, Ecuador: eruptive history, total magma output and potential hazards. *Journal of*  
931 *South American Earth Sciences*, 106, 103046.

932 Bablon, M., 2018. Reconstruction de l'histoire des volcans de l'arc équatorien: contraintes pour  
933 l'évolution chronologique de l'arc andin et pour l'évaluation du risque volcanique (Doctoral  
934 dissertation, Paris Saclay).

935 Bablon, M., Quidelleur, X., Samaniego, P., Le Pennec, J. L., Audin, L., Jomard, H., Alvarado, A.,  
936 2019. Interactions between volcanism and geodynamics in the southern termination of the  
937 Ecuadorian arc. *Tectonophysics*, 751, 54-72.

938 Bablon, M., Quidelleur, X., Samaniego, P., Le Pennec, J. L., Lahitte, P., Liorzou, C., Hidalgo, S.,  
939 2018. Eruptive chronology of Tungurahua volcano (Ecuador) revisited based on new K-Ar ages  
940 and geomorphological reconstructions. *Journal of Volcanology and Geothermal Research*, 357,  
941 378-398.

942 Bablon, M., Quidelleur, X., Samaniego, P., Le Pennec, J. L., Santamaría, S., Liorzou, C., Eschbach,  
943 B., 2020. Volcanic history reconstruction in northern Ecuador: insights for eruptive and erosion  
944 rates on the whole Ecuadorian arc. *Bulletin of Volcanology*, 82(1), 1-23.

945 Baize, S., Audin, L., Alvarado, A., Jomard, H., Bablon, M., Champenois, J., Le Pennec, J. L., 2020a.  
946 Active 961 Tectonics and Earthquake Geology Along the Pallatanga Fault, Central Andes of  
947 Ecuador. *Frontiers in Earth Science*, 8, 193.

948 Baize, S., Nurminen, F., Sarmiento, A., Dawson, T., Takao, M., Scotti, O., Civico, R., 2020b. A  
949 worldwide and Unified Database of Surface Ruptures (SURE) for fault displacement hazard  
950 analyses. *Seismological Research Letters*, 91(1), 499-520.

951 Barberi, F., Coltelli, M., Ferrara, G., Innocenti, F., Navarro, J. M., Santacroce, R., 1988. Plio-  
952 quaternary volcanism in Ecuador. *Geological Magazine*, 125(1), 1-14.

953 Beauval, C., Yepes, H., Bakun, W. H., Egred, J., Alvarado, A., Singaicho, J. C., 2010. Locations and  
954 magnitudes of historical earthquakes in the Sierra of Ecuador (1587–1996). *Geophysical Journal*  
955 *International*, 181(3), 1613-1633.

956 Bellver-Baca, M. T., Chiaradia, M., Beate, B., Beguelin, P., Deriaz, B., Mendez-Chazarra, N.,  
957 Villagómez, D., 2020. Geochemical evolution of the Quaternary Chachimbiro Volcanic Complex  
958 (frontal volcanic arc of Ecuador). *Lithos*, 356, 105237.

959 Bernard, B., & Andrade, D. (2011). Volcanes cuaternarios del Ecuador continental. *IGEPN Poster*  
960 *Informativo*.

961 Bernard, B., Hidalgo, S., Robin, C., Beate, B., Quijozaca, J., 2014. The 3640–3510 BC rhyodacite  
962 eruption of Chachimbiro compound volcano, Ecuador: a violent directed blast produced by a  
963 satellite dome. *Bulletin of Volcanology*, 76(9), 1-20.

964 Boland, M.P., McCourt, W.J., Beate, B., 2000. Mapa geológico de la Cordillera Occidental del  
965 Ecuador entre 08–s18N, escala 1/200.000. British Geological Survey-CODIGEM, Dirección  
966 Nacional de Geología, Quito.

967 Bourgois, J., 2013. A review on tectonic record of strain buildup and stress release across the Andean  
968 forearc along the gulf of Guayaquil-Tumbes basin (GGTB) near Ecuador-Peru  
969 border. *International Journal of Geosciences*, 4, 618-635.

970 Cassagnol, C., Gillot, P.-Y., 1982. Range and effectiveness of unspiked potassium-argon dating:  
971 experimental groundwork and application. *Odin GS Ed Numer. Dating Stratigr.* John Wiley & Sons,  
972 New York, 159–179.

973 Clapperton, C. M., 1990. Glacial and volcanic geomorphology of the Chimborazo-Carihuairazo  
974 massif, Ecuadorian Andes. *Earth and Environmental Science Transactions of the Royal Society*  
975 *of Edinburgh*, 81(2), 91-116.

976 Cole, J. W., Milner, D. M., Spinks, K. D., 2005. Calderas and caldera structures: a review. *Earth-*  
977 *Science Reviews*, 69(1-2), 1-26.

978 Cotten, J., Le Dez, A., Bau, M., Caroff, M., Maury, R. C., Dulski, P., Brousse, R., 1995. Origin of  
979 anomalous rare-earth element and yttrium enrichments in subaerially exposed basalts: evidence  
980 from French Polynesia. *Chemical Geology*, 119(1-4), 115-138.

981 Deino, A., Potts, R., 1992. Age-probability spectra for examination of single-crystal <sup>40</sup>Ar/<sup>39</sup>Ar dating  
982 results: Examples from Olorgesailie, southern Kenya Rift. *Quaternary International*, 13, 47-53.

983 Deligne, N. I., Coles, S. G., Sparks, R. S. J., 2010. Recurrence rates of large explosive volcanic  
984 eruptions. *Journal of Geophysical Research: Solid Earth*, 115(B6).

985 Deline, P. (2009). Interactions between rock avalanches and glaciers in the Mont Blanc massif during  
986 the late Holocene. *Quaternary Science Reviews*, 28(11-12), 1070-1083.

987 Dibacto Kamwa, S., 2020. Dynamique de construction et démantèlement des volcans tertiaires et  
988 quaternaires des Carpates par des approches géomorphologiques et géochronologiques  
989 (Doctoral dissertation, université Paris-Saclay).

990 Dufresne, A., Siebert, L., Bernard, B., 2021. Distribution and geometric parameters of volcanic debris-  
991 avalanche deposits. In *Volcanic Debris Avalanches* (pp. 75-90). Springer, Cham.

992 Ego, F., Sébrier, M., Carey-Gailhardis, E., Beate, B., 1996. Do the Billecocha normal faults (Ecuador)  
993 reveal extension due to lithospheric body forces in the northern Andes?. *Tectonophysics*, 265(3-  
994 4), 255-273.

995 Ego, F., Sébrier, M., Lavenu, A., Yepes, H., Egues, A., 1996. Quaternary state of stress in the  
996 Northern Andes and the restraining bend model for the Ecuadorian  
997 Andes. *Tectonophysics*, 259(1-3), 101-116.

998 Egeuz, A., Alvarado, A., Yepes, H., Machette, M. N., Costa, C., Dart, R. L., Bradley, L. A., 2003.  
999 Database and map of Quaternary faults and folds of Ecuador and its offshore regions. US  
1000 Geological Survey Open-File Report, 3, 289. doi=10.1.1.593.980

1001 Feininger, T., Bristow, C. R., 1980. Cretaceous and Paleogene geologic history of coastal  
1002 Ecuador. *Geologische Rundschau*, 69(3), 849-874.

1003 Germa, A., Lahitte, P., Quidelleur, X., 2015 Construction and destruction of Mont Pelée volcano:  
1004 volumes and rates constrained from a geomorphological model of evolution: construction and  
1005 destruction of Mont Pelée. *J Geophys Res Earth Surf* 120:1206–1226.  
1006 <https://doi.org/10.1002/2014JF003355>

1007 Germa, A., Quidelleur, X., Lahitte, P., Labanieh, S., Chauvel, C., 2011. The K–Ar Cassagnol– Gillot  
1008 technique applied to western Martinique lavas: A record of Lesser Antilles arc ACCEPTED  
1009 MANUSCRIPT ACCEPTED MANUSCRIPT 32 activity from 2 Ma to Mount Pelée volcanism. *Quat.*  
1010 *Geochronol.* 6, 341–355.

1011 Gillot, P.-Y., Hildenbrand, A., Lefèvre, J.-C., Albore-Livadie, C., 2006. The K/Ar dating method:  
1012 principle, analytical techniques, and application to Holocene volcanic eruptions in Southern Italy.  
1013 *Acta Vulcanol.* 18, 55–66.

1014 Goossens, P. J., Rose Jr, W. I., 1973. Chemical composition and age determination of tholeiitic rocks  
1015 in the basic igneous complex, Ecuador. *Geological Society of America Bulletin*, 84(3), 1043-1052.

1016 Guillier, B., Chatelain, J. L., Jaillard, E., Yepes, H., Poupinet, G., Fels, J. F., 2001. Seismological  
1017 evidence on the geometry of the orogenic system in central-northern Ecuador (South  
1018 America). *Geophysical Research Letters*, 28(19), 3749-3752.

1019 Gunkel, G., Beulker, C., 2009. Limnology of the Crater Lake Cuicocha, Ecuador, a cold-water tropical  
1020 lake. *International Review of Hydrobiology*, 94(1), 103-125.

1021 Gunkel, G., Beulker, C., Grupe, B., Viteri, F., 2009. Survey and assessment of post volcanic activities  
1022 of a young caldera lake, Lake Cuicocha, Ecuador. *Natural Hazards and Earth System*  
1023 *Sciences*, 9(3), 699.

1024 Gutscher, M.-A., J., Malavieille, S., Lallemand., J.-Y., Collot, 1999, Tectonic segmentation of the  
1025 North Andean margin: Impact of the Carnegie Ridge collision, *Earth Planet. Sci. Lett.*, 168(3), 255–  
1026 270.

1027 Hall, M. L., Mothes, P. A., 1994. Tefroestratigrafía holocénica de los volcanes principales del valle  
1028 interandino, Ecuador. *Estudios de geografía*, 6, 47-67.

1029 Hall, M. L., & Wood, C. A. (1985). Volcano-tectonic segmentation of the northern Andes. *Geology*,  
1030 13(3), 203-207.

1031 Hall, M. L., Mothes, P. A., Samaniego, P., Militzer, A., Beate, B., Ramón, P., Robin, C., 2017. Antisana  
1032 volcano: a representative andesitic volcano of the eastern cordillera of Ecuador: petrography,  
1033 chemistry, tephra, and glacial stratigraphy. *Journal of South American Earth Sciences*, 73, 50-64.

1034 Hall, M. L., Robin, C., Beate, B., Mothes, P., Monzier, M., 1999. Tungurahua Volcano, Ecuador:  
1035 structure, eruptive history, and hazards. *Journal of Volcanology and Geothermal Research*, 91(1),  
1036 1-21.

1037 Hall, M. L., Samaniego, P., Le Pennec, J. L., Johnson, J. B., 2008. Ecuadorian Andes volcanism: A  
1038 review of Late Pliocene to present activity. *Journal of Volcanology and Geothermal  
1039 Research*, 176(1), 1-6.

1040 Hall, M., Mothes, P., 2008. The rhyolitic–andesitic eruptive history of Cotopaxi volcano,  
1041 Ecuador. *Bulletin of Volcanology*, 70(6), 675-702.

1042 Hall, M., Ramón, P., Mothes, P., Le Pennec, J. L., García, A., Samaniego, P., Yepes, H., 2004.  
1043 Volcanic eruptions with little warning: the case of Volcán Reventador's Surprise November 3, 2002  
1044 Eruption, Ecuador. *Revista geológica de Chile*, 31(2), 349-358.

1045 Harford, C.L., Pringle, M.S., Sparks, R.S.J., Young, S.R., 2002. The volcanic evolution of Montserrat  
1046 using  $^{40}\text{Ar}/^{39}\text{Ar}$  geochronology. *Geol. Soc. Lond. Mem.* 21, 93–113.

1047 Hidalgo, S., Gerbe, M. C., Martin, H., Samaniego, P., Bourdon, E., 2012. Role of crustal and slab  
1048 components in the Northern Volcanic Zone of the Andes (Ecuador) constrained by Sr–Nd–O  
1049 isotopes. *Lithos*, 132, 180-192.

1050 Hidalgo, S., Monzier, M., Almeida, E., Chazot, G., Eissen, J. P., van der Plicht, J., Hall, M. L., 2008.  
1051 Late Pleistocene and Holocene activity of the Atacazo–Ninahuilca volcanic complex  
1052 (Ecuador). *Journal of Volcanology and Geothermal Research*, 176(1), 16-26.

1053 Hughes, R. A., Pilatasig, L. F., 2002. Cretaceous and Tertiary terrane accretion in the Cordillera  
1054 Occidental of the Andes of Ecuador. *Tectonophysics*, 345(1-4), 29-48.

1055 Jaillard, E., Ordonez, M., Suarez, J., Toro, J., Iza, D., Lugo, W., 2004. Stratigraphy of the Late  
1056 Cretaceous–Paleogene deposits of the cordillera occidental of central Ecuador: geodynamic  
1057 implications. *Journal of South American Earth Sciences*, 17(1), 49-58.

1058 Jomard, H., Saqui, D., Baize, S., Alvarado, A., Bernard, B., Audin, L., Hidalgo, S., Pacheco, D., Ruiz,  
1059 M., Segovia, M., 2021. Interactions between active tectonics and gravitational deformation along  
1060 with the Billecocha fault system (Northern Ecuador): Insights from morphological and  
1061 paleoseismological investigations, *Journal of South American Earth Sciences*. DOI: [HTTPS://  
1062 doi.org/10.1016/j.jsames.2021.103406](https://doi.org/10.1016/j.jsames.2021.103406).

1063 Kerr, A. C., Aspden, J. A., Tarney, J., Pilatasig, L. F., 2002. The nature and provenance of accreted  
1064 oceanic terranes in western Ecuador: geochemical and tectonic constraints. *Journal of the*  
1065 *Geological Society*, 159(5), 577-594.

1066 Lahitte, P., Samper, A., Quidelleur, X., 2012. DEM-based reconstruction of southern Basse-Terre  
1067 volcanoes (Guadeloupe archipelago, FWI): Contribution to the Lesser Antilles Arc construction  
1068 rates and magma production. *Geomorphology*, 136(1), 148-164.

1069 Lara, L. E., 2009. The 2008 eruption of the Chaitén Volcano, Chile: a preliminary report. *Andean*  
1070 *Geology*, 36(1), 125-129.

1071 Le Pennec, J. L., Ruiz, A. G., Eissen, J. P., Hall, M. L., Fornari, M., 2011. Identifying potentially active  
1072 volcanoes in the Andes: Radiometric evidence for late Pleistocene-early Holocene eruptions at  
1073 Volcán Imbabura, Ecuador. *Journal of Volcanology and Geothermal Research*, 206(3-4), 121-  
1074 135.

1075 Legros, F., 2000. Minimum volume of a tephra fallout deposit estimated from a single isopach. *Journal*  
1076 *of Volcanology and Geothermal Research*, 96(1-2), 25-32.

1077 Lipman, P. W. (2000). Calderas. *Encyclopedia of volcanoes*, 643-662.

1078 Lonsdale, P., 2005. Creation of the Cocos and Nazca plates by fission of the Farallon plate,  
1079 *Tectonophysics*, 404(3-4), 237–264, doi:10.1016/j.tecto.2005.05.011.

1080 Luzieux, L. D. A., Heller, F., Spikings, R., Vallejo, C. F., Winkler, W., 2006. Origin and Cretaceous  
1081 tectonic history of the coastal Ecuadorian forearc between 1 N and 3 S: Paleomagnetic,  
1082 radiometric and fossil evidence. *Earth and Planetary Science Letters*, 249(3-4), 400-414.

1083 Madera, L. F., 1918. Ibarra y el terremoto de 1868.

1084 Melián, G. V., Toulkeridis, T., Pérez, N. M., Hernández, P. A., Somoza, L., Padrón, E., Cordero, M.,  
1085 2021. Geochemistry of Water and Gas Emissions from Cuicocha and Quilotoa Volcanic Lakes,  
1086 Ecuador. *Front. Earth Sci*, 9, 741528.

1087 Michaud, F., C. Witt., J. Y. Royer., 2009, Influence of the subduction of the Carnegie volcanic ridge  
1088 on Ecuadorian geology: Reality and fiction, *Geol. Soc. Jpn. Mem.*, 204, 217–228,  
1089 doi:10.1130/2009.1204(10).

1090 Monzier, M., Robin, C., Samaniego, P., Hall, M. L., Cotten, J., Mothes, P., Arnaud, N., 1999. Sangay  
1091 volcano, Ecuador: structural development, present activity, and petrology. *Journal of Volcanology*  
1092 *and Geothermal Research*, 90(1-2), 49-79.

1093 Navarrete, W.F., Le Pennec, J.L., Solano, S., Liorzou, C., Ruiz, G.A., 2020. A first reconstruction of  
1094 the evolution of Cubilche Volcanic complex, Imbabura Province, Ecuador. *J. Volcanol. Geotherm.*  
1095 *Res.* 406, 107023 <https://doi.org/10.1016/j.jvolgeores.2020.107023>.

1096 Newhall, C. G., & Punongbayan, R. (Eds.), 1996. Fire and mud: eruptions and lahars of Mount  
1097 Pinatubo, Philippines (p. 1126). Quezon City: Philippine Institute of Volcanology and Seismology.

1098 Newhall, C.G., Self, S., 1982. The volcanic explosivity index (VEI) an estimate of explosive magnitude  
1099 for historical volcanism. *J. Geophys. Res.: Oceans* 87, 1231–1238.



1100 Nocquet, J. M., Villegas-Lanza, J. C., Chlieh, M., Mothes, P. A., Rolandone, F., Jarrin, P., Yepes, H.,  
1101 2014. Motion of continental slivers and creeping subduction in the northern Andes. *Nature*  
1102 *Geoscience*, 7(4), 287-291.

1103 Peccerillo, A., Taylor, S.R., 1976. Geochemistry of Eocene calc-alkaline volcanic rocks from the  
1104 Kastamonu area, northern Turkey. *Contrib. Mineral. Petrol.* 58, 63–81.

1105 Picuasi, S., Julio, C. 2013. Aportes al Ordenamiento Territorial desde la cosmovisión de los pueblos  
1106 originarios (Bachelor's thesis).

1107 Pidgen, A., 2014. Cuicocha Volcano, Ecuador: reconstruction of major explosive phases through  
1108 investigation of associated pyroclastic deposits. Trinity: University of Oxford (Master's thesis).

1109 Pratt, W. T., Duque, P., Ponce, M., 2005. An autochthonous geological model for the eastern Andes  
1110 of Ecuador. *Tectonophysics*, 399(1-4), 251-278.

1111 Punongbayan, R. S., Newhall, C. G., Hoblitt, R. P., 1996. Photographic record of rapid geomorphic  
1112 change at Mount Pinatubo, 1991–94. *Fire and Mud: Eruptions and Lahars of Mount Pinatubo,*  
1113 *Philippines*, 21-66.

1114 Reimer, P. J. 2020. Composition and consequences of the IntCal20 radiocarbon calibration curve.  
1115 *Quaternary Research*, 96, 22-27.

1116 Reimer, P. J., Bard, E., Bayliss, A., Beck, J. W., Blackwell, P. G., Ramsey, C. B., Van Der Plicht, J.,  
1117 2013. IntCal13 and Marine13 radiocarbon age calibration curves 0–50,000 years cal  
1118 BP. *radiocarbon*, 55(4), 1869-1887.

1119 Ricci, J., Lahitte, P., Quidelleur, X., 2015a. Construction and destruction rates of volcanoes within  
1120 tropical environment: Examples from the Basse-Terre Island (Guadeloupe, Lesser Antilles).  
1121 *Geomorphology* 228, 597–607.

1122 Ricci, J., Quidelleur, X., Lahitte, P., 2015b. Volcanic evolution of central Basse-Terre Island revisited  
1123 on the basis of new geochronology and geomorphology data. *Bull. Volcanol.* 77.

1124 Robin, C., Samaniego, P., Le Pennec, J. L., Fornari, M., Mothes, P., Van Der Plicht, J., 2010. New  
1125 radiometric and petrological constraints on the evolution of the Pichincha volcanic complex  
1126 (Ecuador). *Bulletin of volcanology*, 72(9), 1109-1129.

1127 Robin, C., Samaniego, P., Le Pennec, J.L., Fornari, M., Mothes, P., van der Plicht, J., 2010. New  
1128 radiometric and petrological constraints on the evolution of the Pichincha volcanic complex  
1129 (Ecuador). *Bull. Volcanol.* 72, 1109–1129. <http://dx.doi.org/10.1007/s00445-010-0389-0>

1130 Roverato, M., Dufresne, A., Procter, J., 2021. Volcanic Debris Avalanches.

1131 Roverato, M., Larrea, P., Casado, I., Mulas, M., Béjar, G., Bowman, L., 2018. Characterization of the  
1132 Cubilche debris avalanche deposit, a controversial case from the northern Andes,  
1133 Ecuador. *Journal of Volcanology and Geothermal Research*, 360, 22-35.

1134 Samaniego, P., Barba, D., Robin, C., Fornari, M., Bernard, B., 2012. Eruptive history of Chimborazo  
1135 volcano (Ecuador): A large, ice-capped and hazardous compound volcano in the Northern  
1136 Andes. *Journal of Volcanology and Geothermal Research*, 221, 33-51.

1137 Samaniego, P., Martin, H., Monzier, M., Robin, C., Fornari, M., Eissen, J. P., Cotten, J., 2005.  
1138 Temporal evolution of magmatism in the Northern Volcanic Zone of the Andes: the geology and  
1139 petrology of Cayambe Volcanic Complex (Ecuador). *Journal of petrology*, 46(11), 2225-2252.

1140 Samaniego, P., Monzier, M., Robin, C., Hall, M. L., 1998. Late Holocene eruptive activity at Nevado  
1141 Cayambe Volcano, Ecuador. *Bulletin of Volcanology*, 59(7), 451-459.

1142 Samaniego, P., Rivera, M., Mariño, J., Guillou, H., Liorzou, C., Zerathe, S., Scao, V., 2016. The  
1143 eruptive chronology of the Ampato–Sabancaya volcanic complex (Southern Peru). *Journal of*  
1144 *Volcanology and Geothermal Research*, 323, 110-128.

1145 Samaniego, P., Ordóñez, J., Bablon, M., Hall, M. L., Quidelleur, X., Lahitte, P., Liorzou, C., 2022. The  
1146 eruptive chronology of the Carihuairazo volcano (Ecuador): Recurrent sector collapses of a Middle  
1147 Pleistocene stratovolcano of the northern andes. *Journal of South American Earth Sciences*, 116,  
1148 103865.

1149 Samper, A., Quidelleur, X., Lahitte, P., Mollex, D., 2007. Timing of effusive volcanism and collapse  
1150 events within an oceanic arc island: Basse-Terre, Guadeloupe archipelago (Lesser Antilles Arc).  
1151 *Earth Planet. Sci. Lett.* 258, 175–191.

1152 Satake, K., Kate, Y., 2001. The 1741 Oshima-Oshima eruption: extent and volume of submarine  
1153 debris avalanche. *Geophys Res Lett* 28(3):427–430

1154 Sierra, D., Hidalgo, S., Almeida, M., Vigide, N., Lamberti, M. C., Proaño, A., Narváez, D. F., 2021.  
1155 Temporal and spatial variations of CO<sub>2</sub> diffuse volcanic degassing on Cuicocha Caldera Lake–  
1156 Ecuador. *Journal of Volcanology and Geothermal Research*, 411, 107145.

1157 Singer, B. S., Wijbrans, J. R., Nelson, S. T., Pringle, M. S., Feeley, T. C., Dungan, M. A., 1998.  
1158 Inherited argon in a Pleistocene andesite lava: <sup>40</sup>Ar/<sup>39</sup>Ar incremental-heating and laser-fusion  
1159 analyses of plagioclase. *Geology*, 26(5), 427-430.

1160 Spikings, R. A., Winkler, W., Hughes, R. A., Handler, R., 2005. Thermochronology of allochthonous  
1161 terranes in Ecuador: Unravelling the accretionary and post-accretionary history of the Northern  
1162 Andes. *Tectonophysics*, 399(1-4), 195-220.

1163 Stuiver, M., Reimer, P. J., 1993. Extended 14C database and revised CALIB radiocarbon calibration  
1164 program, *Radiocarbon* 35, 215-230.

1165 Stuiver, M., Reimer, P.J., Reimer, R.W., 2005. CALIB 5.0. [WWW program and documentation].

1166 Sun, S.-s., McDonough, W.F., 1989. Chemical and isotopic systematics of oceanic basalts:  
1167 implications for mantle composition and processes. *Geol. Soc. Lond. Spec. Publ.* 42, 313–345.

1168 Thouret, J.C., Finizola, A., Fornari, M., Suni, J., Legeley-Padovani, A., Frechen, M., 2001. Geology  
1169 of El Misti volcano nearby the city of Arequipa, Peru. *Geol. Soc. Am. Bull.* 113, 1593–1610

1170 Trenkamp, R., Kellogg, J. N., Freymueller, J. T., Mora, H. P., 2002. Wide plate margin deformation,  
1171 southern Central America and northwestern South America, CASA GPS observations. *Journal of*  
1172 *South American Earth Sciences*, 15(2), 157-171.

1173 Troya, R., 1913. Photo from the historical archive of the Central Bank of Ecuador. *Quito, Ecuador.*  
1174 *Code*, 95, F0490.

1175 Troya, R., 1913. Photo from the historical archive of the Central Bank of Ecuador. *Quito, Ecuador.*  
1176 *Code, 95, F0490.*

1177 UN/ISDR ISfDR., 2004. Living with risk: A global review of disaster reduction initiatives, vol 1. United  
1178 Nations Publications, New York and Geneva, URL [http://www.unisdr.org/files/657\\_lwr1.pdf](http://www.unisdr.org/files/657_lwr1.pdf)

1179 Vallejo Vargas, S. X., 2011. *Distribución de las cenizas volcánicas Holocénicas Tardías en la Costa*  
1180 *del Ecuador* (Bachelor's thesis, QUITO/EPN/2011).

1181 Vallejo, C., Almagor, S., Romero, C., Herrera, J. L., Escobar, V., Spikings, R. A., Vermeesch, P.,  
1182 2020. Sedimentology, provenance and radiometric dating of the Silante Formation: Implications  
1183 for the Cenozoic evolution of the Western Andes of Ecuador. *Minerals*, 10(10), 929.

1184 Vallejo, C., Spikings, R. A., Horton, B. K., Luzieux, L., Romero, C., Winkler, W., Thomsen, T. B., 2019.  
1185 Late Cretaceous to Miocene stratigraphy and provenance of the coastal forearc and Western  
1186 Cordillera of Ecuador: Evidence for accretion of a single oceanic plateau fragment. In *Andean*  
1187 *tectonics* (pp. 209-236). Elsevier.

1188 Vallejo, C., Spikings, R. A., Luzieux, L., Winkler, W., Chew, D., Page, L., 2006. The early interaction  
1189 between the Caribbean Plateau and the NW South American Plate. *Terra Nova*, 18(4), 264-269.

1190 Vallejo, C., Winkler, W., Spikings, R. A., Luzieux, L., Heller, F., Bussy, F., 2009. Mode and timing  
1191 of terrane accretion in the forearc of the Andes in Ecuador. *Backbone of the Americas: shallow*  
1192 *subduction, plateau uplift, and ridge and terrane collision*, 204, 197.

1193 Valverde, V., Mothes, P. A., Beate, B., Bernard, J., 2021. Enormous and far-reaching debris  
1194 avalanche deposits from Sangay volcano (Ecuador): Multidisciplinary study and modeling the 30-  
1195 ka sector collapse. *Journal of Volcanology and Geothermal Research*, 411, 107172.

1196 Van Thournout, F., Hertogen, J., Quevedo, L., 1992. Allochthonous terranes in northwestern  
1197 Ecuador. *Tectonophysics*, 205(1-3), 205-221.

1198 Váscquez Müller, A., Cashman, K.V., Mitchell, S.J., Váscquez, F.J., 2022. The 2.6–2.3 ka explosive  
1199 eruptive period of the Pululahua dome complex, Ecuador: insights from pyroclast analysis. *Bull*  
1200 *Volcanol* 84:81. <https://doi.org/10.1007/s00445-022-01590-4>

1201 Voight, B., Glicken, H., Janda, R. J., Douglass, P. M., 1981. Catastrophic rockslide avalanche of May  
1202 18. In: Lipman P.W., Mullineaux D.R. (eds) *The 1980 eruptions of Mount St. Helens*, Washington,  
1203 U.S. Geological Survey Professional Papers 1250:347–377

1204 Von Hillebrandt, C., 1989. Estudio geovolcanológico del Complejo Volcánico Cuicocha-Cotacachi y  
1205 sus aplicaciones. Provincia de Imbabura. Quito: Escuela Politécnica Nacional (Master's thesis).

1206 Von Hillebrandt, C., Hall, M. L., 1988. Mapa de los Peligros Volcánicos Potenciales Asociados con  
1207 el Volcán Cuicocha. *Esc*, 1(50.000).

1208 Whympers, E., 1892. *Travels amongst the Great Andes of the Equator* (Vol. 1). C. Scribner's Sons.

1209 Wilson, M., 1989. Igneous petrogenesis. A global tectonic approach. Chapman and Hall, London,  
1210 Glasgow, New York, Tokyo, Melbourne, Madras., pp. 51-97. ISBN: 0-412-53310-3

1211 Wolf, T., 1892. Geografía y geología del Ecuador; publicada por orden del supremo gobierno de la  
1212 república por Teodoro Wolf. Tipografía de FA Brockhaus.

1213 Yepes, H., Audin, L., Alvarado, A., Beauval, C., Aguilar, J., Font, Y., Cotton, F., 2016. A new view for  
1214 the geodynamics of Ecuador: Implication in seismogenic source definition and seismic hazard  
1215 assessment. *Tectonics*, 35(5), 1249-1279.

1216

1217

1218

1219

1220

1221

1222

1223

1224

1225

1226

1227

1228

1229

1230

1231

1232

1233

1234

1235

1236

1237

1238

1239

1240

1241

1242

1243

1244

1245

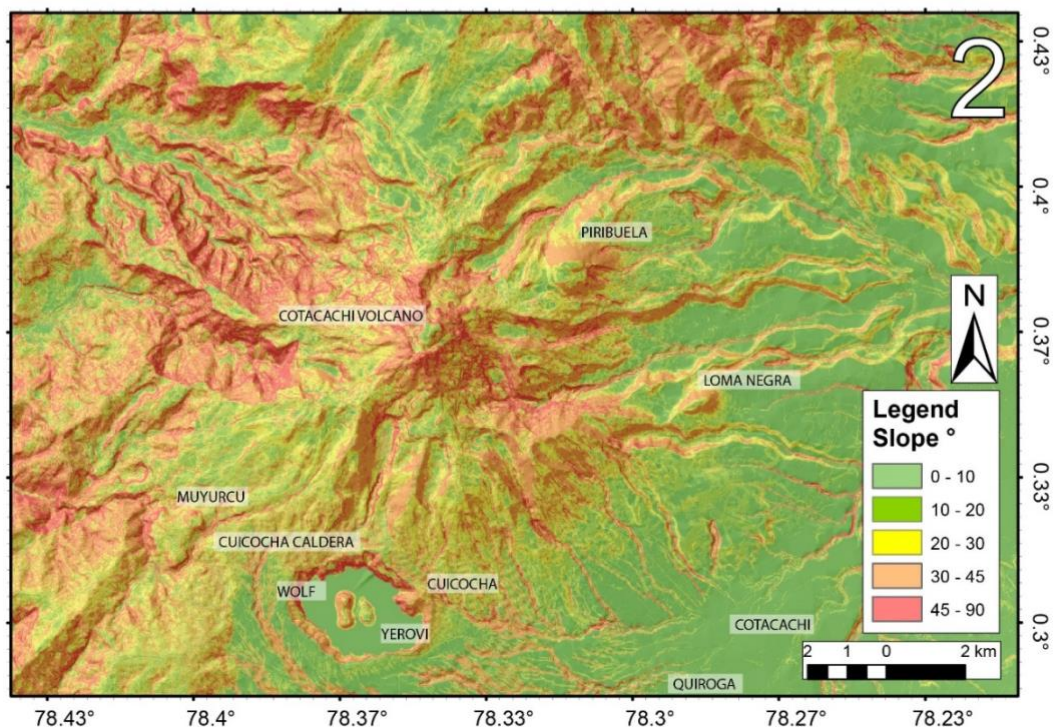
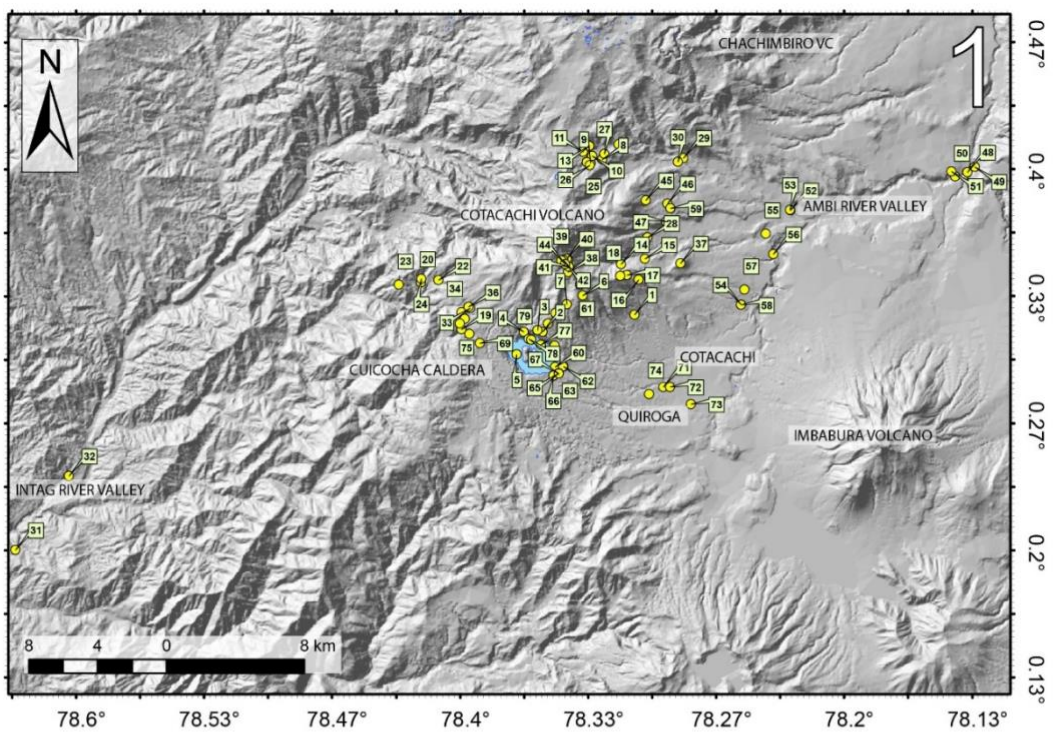
1246

1247

1248

1249

1250



1252

1253

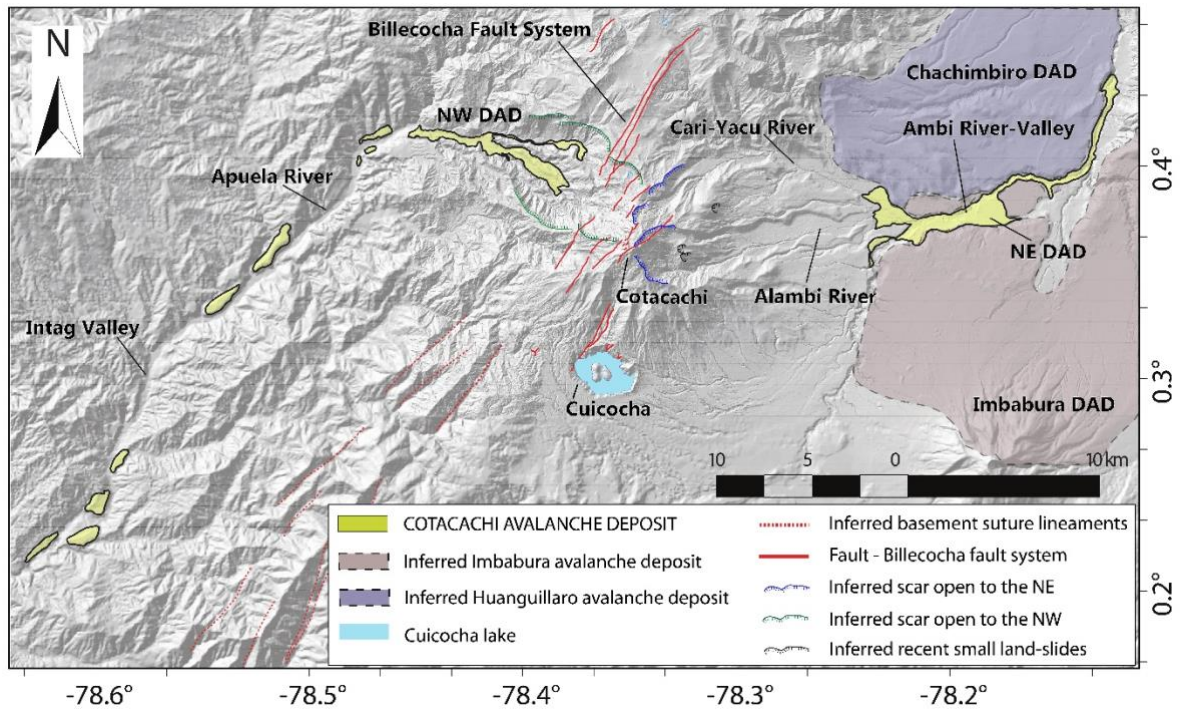
1254

1255

1256

Figure A 1) Field control points of Cotacachi - Cuicocha volcanic complex, for detailed descriptions of each number, see: Table A. 2) Map of slopes of the area of the Cotacachi - Cuicocha volcanic complex. The map was made using five classes based on the angles of inclination of the slope, expressed in degrees (°).

1257



1258

1259

1260

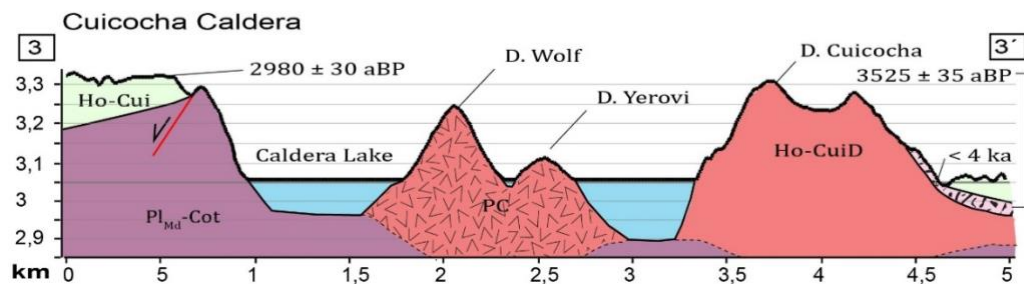
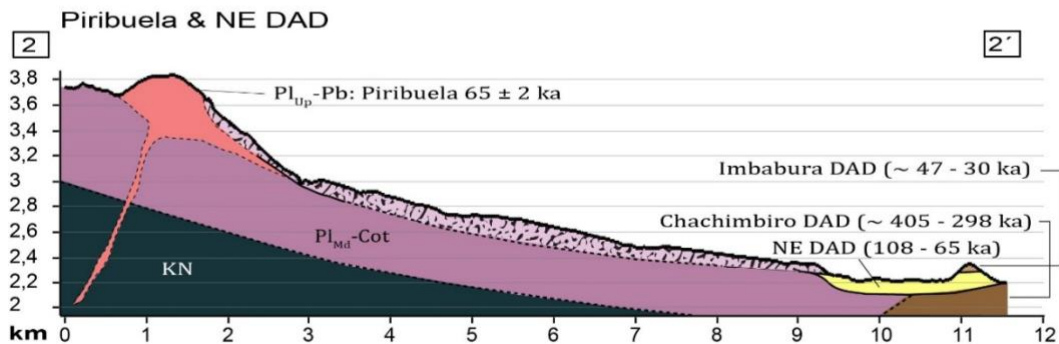
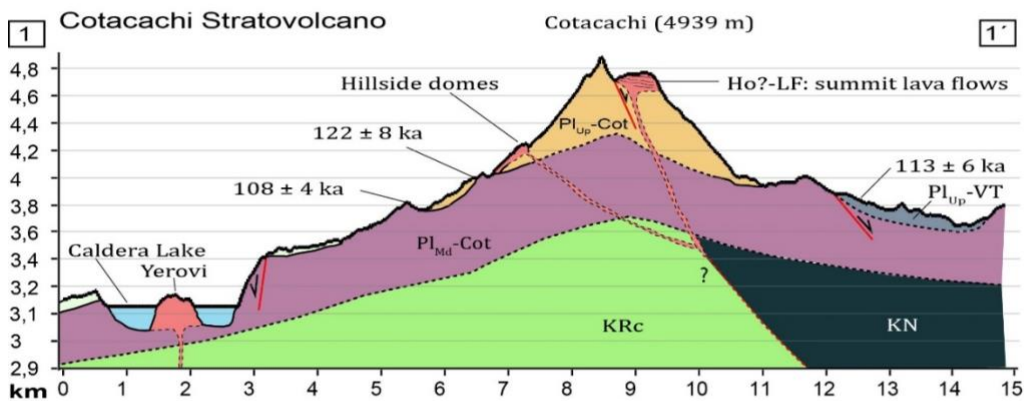
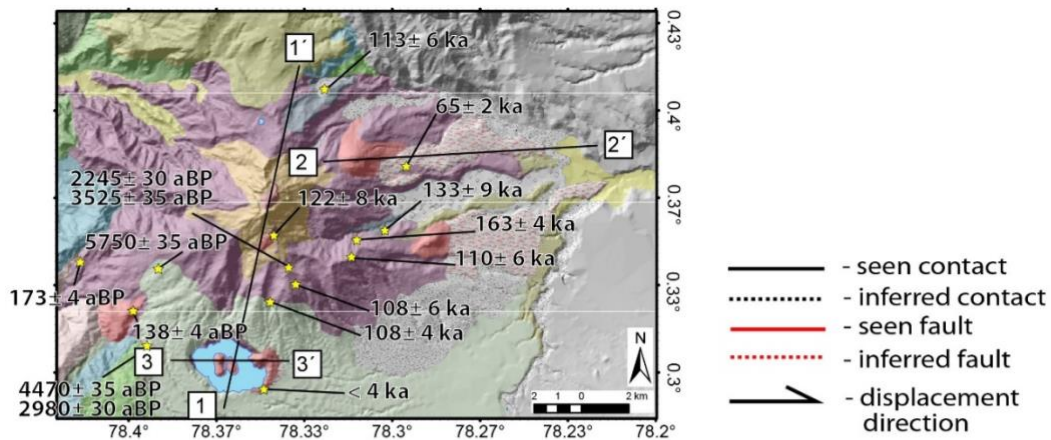
1261

1262

1263

1264

Figure B. Spatial distribution of the mapped NW and NE avalanche deposits (yellow-colored areas) and possible avalanche scars. Note the Billecocha fault system (Ego, 1996; Egeuz et al., 2003; Jomard et al., 2021) crossing the center of the possible avalanche scars. Purple and light brown polygons show the boundaries of the Chachimbiro and Imbabura avalanches. The inferred basement suture lineaments were taken from Boland et al. (2000).



1265

1266

1267

1268

1269

1270

1271

Figure C. Geological profiles show the spatial distribution of the different stratigraphic members and units. The profiles are adjusted to the observations made during the fieldwork and are consistent with the radiometric and radiocarbon ages obtained during the present study. 1) Profile 1-1': NNE-SSW longitudinal section along Cotacachi and Cuicocha. 2) Profile 2-2': Section W-E shows the spatial arrangement of the recent deposits of Piribuela and the avalanche deposits of Cotacachi, Imbabura, and Chachimbiro. 3) Profile 3-3': Section W-E of the Caldera de Cuicocha.